J. metamorphic Geol., 2002, **20,** 493–512

An experimental study of grain scale melt segregation mechanisms in two common crustal rock types

C. W. HOLYOKE, III* AND T. RUSHMER
Department of Geology, University of Vermont, Burlington, VT 05405, USA (trushmer@zoo.uvm.edu)

ABSTRACT Creation of pathways for melt to migrate from its source is the necessary first step for transport of magma to the upper crust. To test the role of different dehydration-melting reactions in the development of permeability during partial melting and deformation in the crust, we experimentally deformed two common crustal rock types. A muscovite-biotite metapelite and a biotite gneiss were deformed at conditions below, at and above their fluid-absent solidus. For the metapelite, temperatures ranged between 650 and 800 °C at $P_c = 700$ MPa to investigate the muscovite-dehydration melting reaction. For the biotite gneiss, temperatures ranged between 850 and 950 °C at $P_c = 1000$ MPa to explore biotite dehydration-melting under lower crustal conditions. Deformation for both sets of experiments was performed at the same strain rate ($\dot{\varepsilon}$) 1.37×10^{-5} s^{-1}. In the presence of deformation, the positive ΔV and associated high dilational strain of the muscovite dehydration-melting reaction produces an increase in melt pore pressure with partial melting of the metapelite. In contrast, the biotite dehydration-melting reaction is not associated with a large dilational strain and during deformation and partial melting of the biotite gneiss melt pore pressure builds more gradually. Due to the different rates in pore pressure increase, melt-enhanced deformation microstructures reflect the different dehydration melting reactions themselves. Permeability development in the two rocks differs because grain boundaries control melt distribution to a greater extent in the gneiss. Muscovite-dehydration melting may develop melt pathways at low melt fractions due to a larger volume of melt, in comparison with biotite-dehydration melting, generated at the solidus. This may be a viable physical mechanism in which rapid melt segregation from a metapelitic source rock can occur. Alternatively, the results from the gneiss experiments suggest continual draining of biotite-derived magma from the lower crust with melt migration paths controlled by structural anisotropies in the protolith.

Key words: dehydration-melting; dilational strain; experimental rock deformation; melt distribution, melt segregation.

INTRODUCTION

The understanding of processes during crustal anatexis has developed significantly over the past decade. Important melt producing reactions can be identified both in the field and in the laboratory (see for example Sawyer, 1987; Vielzeuf & Holloway, 1988; Rushmer, 1991; Rapp & Watson, 1995; Hartel & Pattison, 1996; Pickering & Johnston, 1998; Patiño-Douce & Harris, 1998). There are good conceptual models of how granitic magma is distributed on the grain scale, how it can move through the crust and what drives it (Clemens & Mawer, 1992; Brown & Rushmer, 1997; Brown & Solar, 1998; Gleason *et al*., 1999; Rosenberg & Riller, 2000; Petford *et al.*, 2000), and currently a clearer understanding of the meaning and significance of leucosomes in anatectic terranes is evolving. From detailed chemical and microstructural work in anatectic zones where leucosomes are preserved in various degrees of development, melt distribution and the nature of melt pathways on the grain scale, and the geochemical implications (i.e. whether melts become fractionated or not and at what scale) are slowly becoming unravelled (Weber *et al*., 1985; Weber & Barbey, 1986; Barbey *et al*., 1989; Barbey *et al*., 1990; Barbey *et al*., 1996; Oliver & Barr, 1997; Sawyer, 1998; Brown *et al*., 1999; Solar & Brown, 2001). Most detailed field studies (see Pattison & Hart, 1988; Nyman *et al*., 1995; Sawyer *et al*., 1999; Sawyer, 2001) have looked at the microstructures associated with muscovite, biotite and hornblende dehydration melting at high grade conditions and granite wet melting. These studies are vital to the understanding of the physical nature of melt segregation and the nature of the micropathways. In addition, these studies provide clues to variations in deformation behaviour, bulk permeability, rate of melt pore pressure development and ultimately rate of melt segregation. However, to date there have been no detailed studies on the microstructures associated with partial melting in the muscovite-bearing middle

*Now at Department of Geological Sciences, Brown University, Providence, RI 02906

crustal assemblages. This may not be due to lack of focus on these regions, but because the microstructures are disrupted due the different nature of the muscovite dehydration-melting reaction and the release of H_2O from melts during cooling which subsequently modifies, and destroys, the microstructures (Milord *et al.*, 2001).

Muscovite-dehydration melting alone appears to produce significant change in ΔV over a narrow temperature range, essentially just above the solidus. This is in contrast to the other common crustal hydrous phases, such a biotite, which undergo dehydration melting continuously over a wider temperature interval. In addition, experimental studies under static conditions on muscovite-dehydration melting have shown that the volume change associated with dehydration melting causes a great deal of strain on the framework of the matrix, enough strain to produce melt-filled fractures within grains of quartz and/or feldspar adjacent to muscovite (Connolly *et al.*, 1997). Melt-induced fracturing under static conditions is observed only in muscovite-dehydration melting experiments (Rushmer, 2001). Melt-filled intragrain fractures do not form during biotite-dehydration melting. Calculations showing a negligible volume change and dilational strain also support the conclusion that without applied stress, dehydration melting in biotite will not induce melt fractures; in addition, experimental observations show that melt generation rate is slower and more continuous (Rushmer, 2001).

In this paper, we use experiments to explore the differences between the dehydration melting reactions in muscovite and biotite-bearing natural rocks, but under applied stress. We have used results from the static experiments, which show the distinct differences in dilational strain to test the hypothesis that melt pore pressure is rapidly developed in muscovite-bearing rocks undergoing dehydration melting and that deformation will induce melt-enhanced embrittlement leading to cataclasis close to the solidus. This should contrast with deformation results in biotite-only assemblages where the onset of cataclasis is suppressed due to the slower melt generation rate and the negligible dilational strain associated with dehydration melting. The estimated solidus for the muscovite-dehydration melting is approximately 725 to 780 °C between 700 and 1000 MPa (MBS, Patiño-Douce & Harris, 1998). For the biotite-only assemblage, it is approximately 850 °C between 700 and 1000 MPa, owing to the steep solidus in *P–T* space (Gardien *et al.*, 1995). The melting reactions investigated are:

$$\mathrm{Ms + Qtz + Pl \rightarrow melt + Bt + Als + Kfs},$$

in the metapelite and

$$\mathrm{Bt + Pl + Qtz \rightarrow Opx + Sp + Kfs + melt},$$

in the gneiss. Experiments were performed below, at and above the estimated solidus for each rock. A set of experiments was also performed at two durations at run conditions to further examine melt generation rate.

Below, the specific experimental deformation results on two common crustal rocks, the two-mica metapelite and a biotite gneiss, are presented. The melt distribution, the development of permeability and potential melt pathways produced by deformation during partial melting is then discussed in terms of melt fraction and the specific dehydration-melting reaction. We suggest that melt-enhanced embrittlement may be possible in the middle crust in muscovite-bearing assemblages, allowing rapid segregation of low melt fraction magma, but not as common in the lower crust which is dominated by biotite-only bearing rocks. In biotite-only bearing rocks undergoing partial melting, anisotropy in the protolith may control melt migration pathways in the absence of significant strain.

EXPERIMENTAL STUDY

Experimental methodology

Experiments have been performed on the two rock types to specifically test how volume change (dilational strain) associated with different dehydration melting reactions influences the rate of pore pressure build-up, the development of permeability and potentially, the mechanisms of melt segregation at the grain scale. Microstructures associated with melt-enhanced deformation in the laboratory are dominated by cataclasis because of the accelerated strain rates. However, because experiments on the different starting materials are performed at the same bulk strain rate, we can attempt to eliminate strain rate as a variable and look for subtleties between the different dehydration-melting reactions (high dilation strain vs. low dilational strain). Melt migration through large sections of the samples is not observed, except at the highest melt fractions. Instead melt present zones and associated melt deformation microstructures are evident. These zones are interpreted as sites from which melt must segregate and link melt deformation microstructures at the grain scale with specific dehydration-melting reactions. These observations provide information on possible melt segregation mechanisms. We also compare the development of melt–solid microstructures in the different starting materials at similar melt fractions as possible to eliminate melt fraction as a variable.

Experiments were also conducted at two durations at run conditions prior to deformation. 'Short' experiments were held at conditions for 1 hr before deformation commenced and were performed to investigate the extent of cataclasis in the samples due to pore pressure build up during melting concomitant with deformation. 'Long' experiments were held at conditions for 30 hr before deformation commenced and were performed to test the effect of presence of melt alone on melt-present deformation microstructures. The difference in duration helped to determine, qualitatively, the different rate of melt generation in the two rock types.

Starting materials

The starting materials for this study are a natural greenschist to amphibolite grade muscovite-biotite (two-mica) metapelite (2 M) and a natural biotite-plagioclase-quartz gneiss (BPQ). 2 M is composed of 21% muscovite, 7% biotite, 34% quartz, 25% plagioclase feldspar, 13% K-feldspar and accessory zircon, apatite and monazite. The muscovite and biotite grains are primarily oriented with the {001} cleavage plane parallel to the long axis of the cores. They are free of kinks or other strain features. The quartz grains in the 2 M metapelite have no inclusions and have rare undulatory extinction. Plagioclase

feldspar grains have no inclusions and exhibit no strain features. The K-feldspar grains in this rock have perthitic exsolution and some grains are myrmekitic. These grains are large compared to the quartz and plagioclase grains, but are <0.25 mm across. Samples were cored from a slab of the rock, with foliation parallel to the length of the core. The core lengths were between 15.24 and 12.70 mm and centreless ground for the experiments to a diameter of 6.15 mm (± 0.03 mm). A photomicrograph of the starting material is presented in Fig. 1(a).

The BPQ starting material is composed of 27% biotite, 42% quartz and 31% plagioclase and accessory apatite and titanite. The quartz grains in the starting material have deformation bands and a high degree of undulatory extinction. The plagioclase grains exhibit deformation bands. The {001} plane of biotite is oriented perpendicular to the length of the core, which defines the main foliation. There are a few examples of small biotite grains which are oriented with the {001} plane parallel to the length of the core. The core lengths are between 15.52 and 12.46 mm and centreless ground to a diameter of 6.15 mm (± 0.03 mm) for the experiments. A photomicrograph of the starting material is presented in Fig. 1(b).

The difference in foliation orientation between the two sample types had little effect on the behaviour of the samples with melt present (described in more detail in later sections), but the orientation may have a large effect on the behaviour of the samples under subsolidus conditions. To investigate this difference in behaviour and to compare strengths of the samples, an additional set of experiments was performed by Troeger *et al.* (2001) using cores from the 2 M starting material with the foliation perpendicular to the length of the core. These experiments were performed at the same conditions as two of the experiments performed as part of this study. The results of these experiments will be summarized in the discussion section.

Preparation of assembly materials

At least 12 hr prior to installation in the pressure vessel, the NaCl pieces, furnace, AlSiMag jacket, Pt jacket and discs, thermocouple (type S), sample and zirconia spacers were removed from a dessicator, placed in an oven and dried at 150 °C and 1 atm. One hour prior to installation in the bomb, the NaCl pieces, carbon furnace and AlSiMag jacket were placed in a muffle furnace and dried at 400 °C and 1 atm to remove any possible excess water from the assembly. All materials were removed from the oven and muffle furnace, and installed within the bomb while still hot to the touch to avoid condensation of water in the assembly. The assembly used in this study is shown in Fig. 2.

Experimental procedure

Samples were taken to experiment conditions over a three-hour period. The pressure and temperature conditions were increased to 500 MPa and 500 °C over the first hour and then allowed to remain at those conditions for one hour prior to increasing the pressure and temperature at a rate of *c.* 4.2 MPa min^{-1} and 5 °C min^{-1} to the final experimental conditions. After reaching run conditions the experiments were maintained hydrostatically for either one hour (short experiment) or 30 hr (long experiment) prior to engaging the σ_1 piston. Run conditions of experiments performed are presented in Fig. 3. Deformation of the samples began approximately 1.5 hr after engaging the σ_1 piston. For both the 2 M and BPQ samples there was a time dependence for the amount of melt present at a given P–T condition, but this was much more important in the BPQ samples where long and short experiments at the same P–T conditions produced significantly different melt fractions (1 vs. 20 vol.%). These observations are discussed in further detail below.

After engaging the σ_1 piston, the samples were deformed at an average strain rate ($\dot{\varepsilon}$) of 1.37×10^{-5} s^{-1} for a period of six hours. This was sufficient to shorten (bulk ε) most samples by approximately 20–25%. At the end of each run, the experiment was quenched to room temperature within 1 minute of stopping the σ_1 piston to limit retrograde reaction of phases in the melt, and to preserve melt microstructures. Load and confining pressure were released over a period of approximately 1 hr prior to the removal of the assembly from the bomb. All thin sections were prepared on 1′ discs, cut

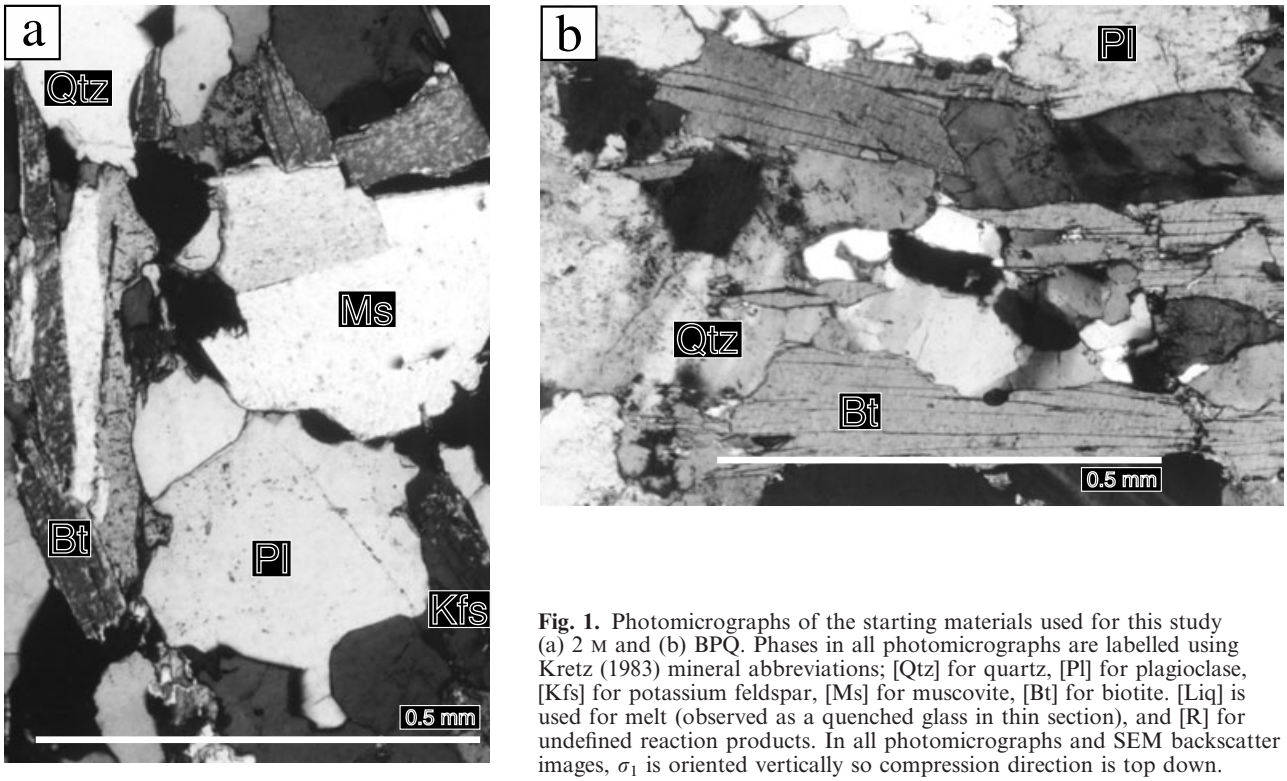

Fig. 1. Photomicrographs of the starting materials used for this study (a) 2 M and (b) BPQ. Phases in all photomicrographs are labelled using Kretz (1983) mineral abbreviations; [Qtz] for quartz, [Pl] for plagioclase, [Kfs] for potassium feldspar, [Ms] for muscovite, [Bt] for biotite. [Liq] is used for melt (observed as a quenched glass in thin section), and [R] for undefined reaction products. In all photomicrographs and SEM backscatter images, σ_1 is oriented vertically so compression direction is top down.

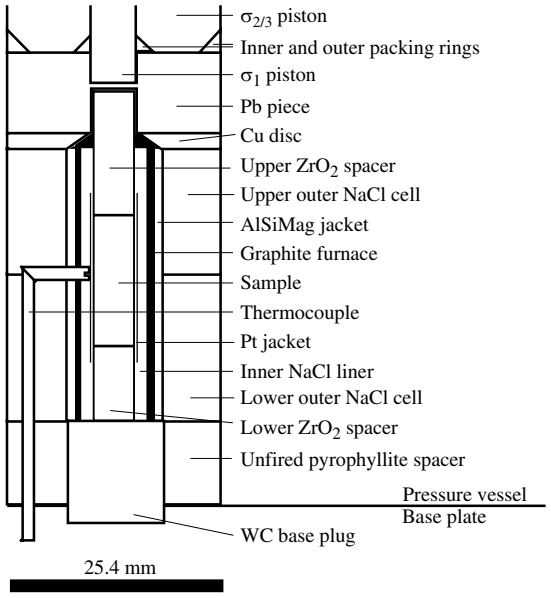

Fig. 2. Schematic representation of the experimental assembly used in this study, which is similar to that used by Kirby & Kronenberg (1984), with modification (shortening) of length of AlSiMag jacket, furnace, upper outer salt, inner salt, and upper spacer. Pt discs (diameter equal to inner diameter of Pt jacket) between the upper spacer/lower spacer and sample are not shown.

parallel to the length of the sample and polished for petrographic and SEM imaging and chemical analysis.

Analytical procedure

All samples were analysed using standard techniques on a petrographic microscope. Photomicrographs of microstructures were collected prior to SEM analysis. For samples with melt or reaction products present, samples were carbon coated and then analysed using a Zeiss SEM for microstructures, mode of phases, melt distribution or evidence of extent of reaction.

In some samples, temperature gradients were observed from the 'hot spot' of the experiment to the top of the sample. This temperature difference is determined by the lack of melt, or lack of evidence of reaction, in the upper regions of the sample, but melt and reaction products were present in the middle and base of the sample, where most strain was accommodated. This is due to a temperature gradient created by the nature of the graphite furnace. To best interpret the experiments deformed in the presence of melt, analysis of the samples was mainly limited to the regions which had melt present. Partitioning of strain into discrete zones was also observed in samples with homogeneously distributed melt. In all experiments, strain is heterogeneously distributed at both the individual-mineral and whole-sample scale and this is attributed to the polymineralic nature of the starting material resulting in heterogeneously distributed deformation. In high melt volume samples it is useful to see how the melt has behaved in the low-strain portions, which developed adjacent to the high strain zones. Strain accommodation heterogeneities at the scale of individual minerals are discussed in each data section, as appropriate. When strain or strain rates of individual samples are discussed (also as shown in Table 1), they refer to the bulk strain and/or strain rates based on the change of sample length parallel to the length of the sample during the experiments. Consequently, bulk strain probably underestimates strain in the melted portion of each sample.

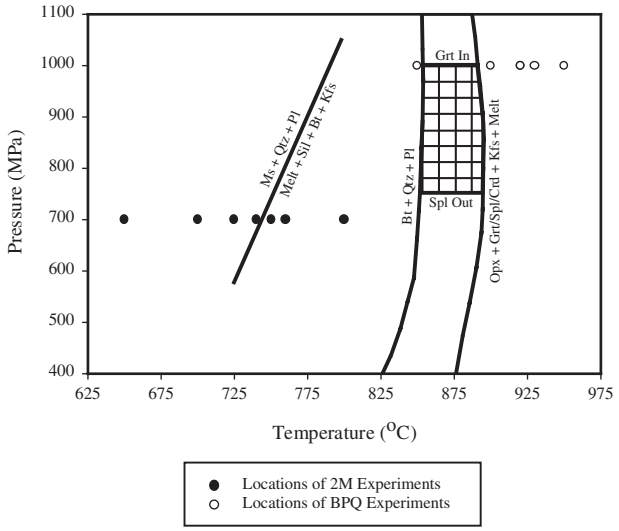

Fig. 3. Location of experimental runs in pressure vs. temperature space. The 2 M experiments performed in this study were all performed at a constant confining pressure of 700 MPa and strain rate of 1.37×10^{-5} s^{-1}. The BPQ experiments were all performed at a constant confining pressure of 1000 MPa and a strain rate of 1.37×10^{-5} s^{-1}. Thus, only the temperature conditions were changed between experiments and this effectively controlled the range of melt fractions studied. Both short and long experiments (see text) were performed on 2 M samples at 725 °C and 740 °C and on BPQ samples at 930 °C. The muscovite dehydration-melting solidus curve is from MBS Patiño-Douce & Harris (1998). Location of biotite-bearing gneiss dehydration melting region is generalized from the experimental results of Patiño-Douce & Beard (1995), Montel & Vielzeuf (1997) and Rushmer, 2001). The lower temperature curve is the solidus (melt-in); the cross-hatched area indicates the region of the spinel-out and garnet-in transition; and the higher temperature curve is biotite-out.

EXPERIMENTAL RESULTS

Sixteen experiments were conducted at conditions which varied from zero to *c.* 40 vol.% (Table 1). Two experiments were conducted to determine the behaviour of each material prior to the onset of dehydration-melting of the respective hydrous phase present (i.e. subsolidus conditions). Six experiments on the 2 M pelite were conducted at conditions of muscovite-dehydration melting (700–740 °C, 700 MPa) to observe the behaviour of the samples at low melt fractions ($\leq$5 vol.%; solidus conditions). Two experiments were conducted at low melt fractions (*c.* 1 vol.%; solidus conditions) using the BPQ material (900–920 °C, 1000 MPa). Four more experiments were conducted at higher melt fractions (up to *c.* 10 vol.% in the 2 M and up to *c.* 20 vol.% in the BPQ material; intermediate melt fraction) to attempt to determine the extent of cataclastic behaviour (750/760 °C, 700 MPa and 920–930 °C, 1000 MPa, respectively) and changes of deformation behaviour with melt fraction. In order to observe behaviour at high melt fraction, one experiment was conducted for each material (*c.* 35 vol.% for

Table 1. List of Experiments Performed.

Exp. No.	Temperature (°C)	Pressure (GPa)	Short/Long	Yield strength (MPa)	Melt fraction (vol.%)	Strain	Effective viscosity (Pa*s)	Comments
2 M-D31	650	0.7	Short	222	0	13%	2.15E+13	Intense kinking of mica grains with some fracturing of quartz and feldspar grains, strain partitioned into mica.
2 M-D29	700	0.7	Long	23	3	24%	1.11E+12	Less focused zone of cataclasis, but the area of cataclastic behaviour is similar to 2 M-D30. Small melt fractures parallel to σ_1 are present in the less strained upper portion of the sample.
2 M-D8	725	0.7	Long	40	1	5%	6.85E+12	Sample exhibits the initial stages of cataclasis, kinking of micas and some fracturing of quartz and feldspar grains away from areas with melt.
2 M-D30	725	0.7	Long	23	3	24%	1.17E+12	Melt lined vertical fractures in upper, less strained portion of the sample. Cataclasis with low melt fraction (*c.* 3 vol.). Partial reaction of muscovite grains and intense fracturing of relic grains of plagioclase and quartz.
2 M-D23	740	0.7	Short	30	3	17%	2.46E+12	Broad cataclastic zone, encompassing lower third of sample. Very little melt observed in upper portion of sample.
2 M-D24	740	0.7	Long	29	5	20%	3.72E+12	Similar features as 2 M-D30, little reaction of muscovite grains in the upper portion of the sample.
2 M-D25	740	0.7	Long	43	5	20%	2.16E+12	Development of intense cataclasis, melt lines some edges of muscovite grains in less strained top section of the sample.
2 M-D20	750	0.7	Short	37	7	21%	1.94E+12	Two zones of cataclasis, one of *c.* 50% grain size reduction and one small zone of *c.* 90% grain size reduction.
2 M-D19	760	0.7	Short	38	9	25%	1.49E+12	Two zones of cataclasis of equal area, one of *c.* 50% grain size reduction and one zone of *c.* 90% grain size reduction.
2 M-D16	800	0.7	Short	60	40	25%	3.54E+12	Very high melt fraction, relic grains of quartz and plagioclase are not fractured, strain is partitioned completely into melt.
BPQ-D52	850	1.0	Long	776	0	14%	8.62E+13	Subsolidus experiment, extension fractures in quartz, fractures along cleavage planes in plagioclase, biotite has undulatory extinction and banding. Through-going faults.
BPQ-D38	900	1.0	Short	723	<1	21%	6.29E+13	Mixed brittle and ductile deformation features. Through-going fractures formed in sample, but partially reacted biotite + reaction products (opx + spinel) have flowed along foliation. The reaction products were not observed during analyses under the petrographic microscope.
BPQ-D40	920	1.0	Short	460	1	13%	4.62E+13	Through-going fractures lined with biotite. No evidence of reaction of biotite grains in thin section. Under SEM analysis melt and reaction products (opx + spl) were observed at the edges of biotite grains which have flowed along grain boundaries.
BPQ-D45	920	1.0	Long	86	20	9%	1.11E+13	Strain is partitioned into melt with little deformation of relic quartz and feldspar grains. Melt pools have formed along the previous foliations in middle of sample, but mixed melt-assisted granular flow and cataclastic behaviour are present at the base of the sample.
BPQ-D41	930	1.0	Short	105	5	13%	9.75E+12	Mixed melt-assisted granular flow and cataclasis with low melt fraction (*c.* 5 vol.%). Strain is partitioned into this region.
BPQ-D32	950	1.0	Short	70	35	24%	1.34E+12	High melt fraction, ductile flow of melt and relic grains, some flow along remnant foliation, with some disturbance of orientation of grains at the base of the sample.

2 M; 800 °C, 700 MPa and *c.* 40 vol.% for BPQ; 950 °C, 1000 MPa; high melt fraction). Each set of experiments (2 M and BPQ) was conducted at a constant confining pressure of either 700 or 1000 MPa. The plots of differential stress vs. strain for the 2 M and the BPQ experiment sets are shown in Fig. 4(a,b), respectively.

Subsolidus conditions

In 2 M experiments conducted under subsolidus conditions (2 M-D31) at 650 °C and 700 MPa, quartz grains are fractured and exhibit undulatory extinction to a greater extent than observed in the starting material. Feldspar grains have fractured along suitably oriented cleavage planes (i.e. oriented at high angle to σ_1), and mica grains are intensely kinked with few undeformed grains. Remaining quartz and feldspar grains appear to be driven into the weaker mica grains along the {001} foliation, demonstrating the relative strength differences of quartz/feldspar and mica at these conditions (Fig. 5a). No through-going faults (faults that extend all the way through the sample) developed in this experimental charge. The differential stress vs. strain curve for this sample reached a peak strength of 222 MPa at 7% bulk strain and weakened

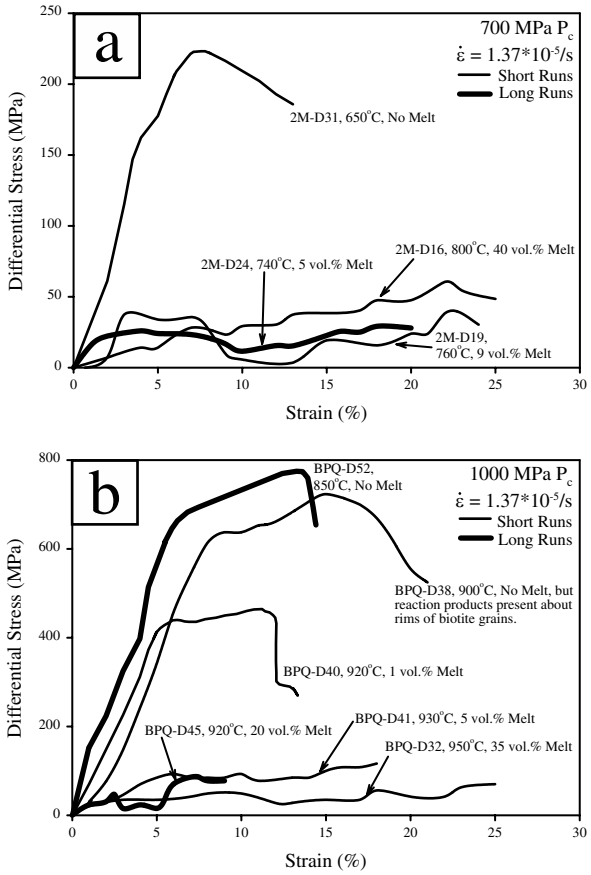

Fig. 4. Graphs of differential stress vs. strain for (a) selected 2 M experiments and (b) all BPQ experiments. (a) All 2 M experiments performed with melt present were weak (<70 MPa) compared to the subsolidus experiment conducted at 650°C, which had a peak strength of 222 MPa and weakened to 187 MPa. No significant pattern of sample behaviour after the initiation of cataclasis is apparent from these curves. For clarity, only three curves representative of the low, medium and high melt fraction behaviours are shown. (b) All BPQ experiments with melt present are weaker than the subsolidus experiment, but unlike the 2 M samples, the BPQ samples gradually weaken as a function of melt fraction up to 5 vol.% melt. At melt fractions equal to and higher than 5 vol.% melt the strengths are essentially the same considering the resolution of load measurement in a solid-medium deformation apparatus.

to a final strength of 185 MPa at 13% bulk strain (Fig. 4a). In this experiment, 2 M was the strongest of all the 2 M experiments performed in this study.

The BPQ experiment conducted at subsolidus/solidus conditions (BPQ-D52) was performed at 850 °C and 1000 MPa and was a long experiment, but no evidence of melting was observed. Three through-going faults developed in this sample, with the greatest displacement along two adjacent faults at the base of the sample. Quartz grains are fractured and have undulatory extinction of equal if not greater intensity than that of the starting material. Plagioclase grains are fractured along cleavage planes (Fig. 6a). Biotite grains are principally fractured and crushed in fault zones or rotated into faults and sheared along {001} planes (Fig. 6b). In some rare instances when small biotite grains are oriented parallel to σ_1 they are moderately kinked (Fig. 6a). Strain was primarily accommodated by the formation of through-going faults (commonly along biotite grains) cutting directly across the sample foliation. The differential stress vs. strain curve increased rapidly to 680 MPa at 5% strain, increased to 776 MPa at 12% strain then failed by faulting at this strain (Fig. 4b).

Low melt fraction experiments

Low melt fraction experiments for the 2 M and BPQ experiments refer to melt fractions up to 5 and 1 vol.%, respectively. The deformation behaviours of the two rock types differ significantly at these low melt fractions. The 2 M samples all developed cataclastic zones, whereas in the BPQ samples the melt and reaction products have moved along grain boundaries and through-going faults have developed.

Six 2 M experiments were conducted at low melt fractions (2 M-D8, 2 M-D23, 2 M-D24, 2 M-D25, 2 M-D29 and 2 M-D30) between 700 and 740 °C (Fig. 3). 2 M-D23 and 2 M-D29 were short experiments, and 2 M-D8, 2 M-D24, 2 M-D25 and 2 M-D30 were all long experiments. In all of these samples, except for 2 M-D8, strain was accommodated by the development of cataclasis in the lower portion of the sample, with *c.* 3 vol.% (2 M-D23, 2 M-D29, 2 M-D30) to *c.* 5 vol.% (2 M-D24 and 2 M-D25) melt present in these zones. Because 2 M-D8 was only strained 5%, little cataclasis was observed, but occurred in small zones about partially reacted muscovite grains. In all of the samples most grains in the upper portions of the samples were not highly fractured, but muscovite and biotite grains are kinked. In the samples with the most uniform melt distribution throughout (2 M-D29 and 2 M-D30), vertical, melt-filled cracks developed through quartz and feldspar grains above partially reacted, unkinked, muscovite grains (Fig. 7a). In the sample from experiment 2 M-D23 the cataclasis was pervasive, encompassing the entire bottom third of the sample. In both 2 M-D24 and 2 M-D25, the cataclastic zones are located in the lower half of the sample and there is a triangular region at the base which has few fractures or other brittle deformation features, and in general similar to the upper portion of the sample; this may be a piston effect, focusing deformation into the weakest zone of the sample. The differential stress vs. strain for these samples is presented in Fig. 4(a).

Partially reacted muscovite grains with solid reaction products (alumino-silicate plus biotite and sometimes K-feldspar), melt (glass) and intensely fractured plagioclase and quartz grains (Fig. 7b) are observed in the cataclastic regions of 2 M-D24 and 2 M-D25. Original biotite is kinked and in some cases partially

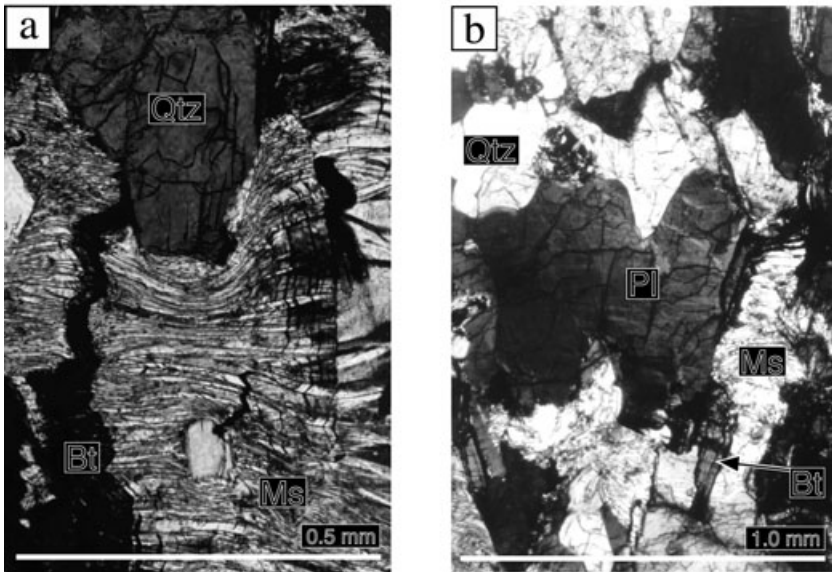

Fig. 5. Photomicrographs (cross nichols) show kinking of micas and fracturing of quartz/feldspar grains in 2 M-D31 (T=650 °C). (a) The quartz grain has been driven into the muscovite and biotite grains. This has caused extreme kinking at the interface between the two phases, the intensity of which decreases away from the interface between the two grains. The right side of the muscovite grain is only slightly kinked compared to the centre. (b) Plagioclase grain which has undergone fracturing.

disintegrated by intense deformation. In these samples, the upper portions were relatively undeformed; some kinking of mica grains and rare fractures in quartz and feldspar grains were observed. Strain was accommodated partially by the kinking of mica but primarily by the cataclastic zones formed during deformation and partial melting.

Experiments BPQ-D38 and BPQ-D40 were conducted at 900 and 920 °C/1000 MPa, using the BPQ material at conditions above the solidus estimated from the static experimental results (850 °C). These short experiments produced observable reaction products around the edges of biotite grains at 900 °C and melt plus solid reaction products (orthopyroxene plus spinel) at 920 °C. In both experiments, partially reacted biotite grains and the reaction products located at the sites of reaction appeared to have flowed along the quartz and feldspar grain boundaries, following the foliation. Through-going faults are also observed in these samples. The differential stress vs. strain curve for run BPQ-D38 shows a decrease in strength starting at 15% strain (Fig. 4b). This sample lost strength through a combination of flow of biotite and reaction products and conjugate sets of through-going fractures which are filled with finely ground biotite grains and solid reaction products. The individual minerals outside of these faults are highly deformed, especially the biotite grains. Figure 8(a) shows these areas of finely disrupted biotite grains. SEM analyses show that orthopyroxene grains have formed along the edges of the biotite grains, indicating that the biotite has reacted, possibly generating melt (Fig. 8a), although no glass was observed. However, melt and solid reaction products are observed in thin section from sample BPQ-D40 (920 °C/1000 MPa, Fig. 8b). In both experiments, the partially reacted biotite grains and the reaction products and melt have migrated around quartz and plagioclase grains.

Intermediate melt fraction experiments

2 M-D19 and 2 M-D20 were conducted at 760 and 750 °C, respectively, so to produce intermediate melt fractions (*c.* 10 vol.% in 2 M-D19 and *c.* 7 vol.% in 2 M-D20). Both of these samples exhibit cataclasis; however, two regions of different intensities of cataclasis are observed (Table 1). Individual minerals within the cataclastic zones in both of the samples behave as in the experiments at 740 °C, with intense fracturing of quartz and feldspar producing angular grains and kinking in mica. The grain size reduction in the zones of cataclasis can be divided into two regions, one region of approximately 50% grain size reduction and one region of 90% grain size reduction. The strengths of these samples are very similar to the strengths of the experiments with lower melt fractions.

Two BPQ experiments were conducted with melt fractions of *c.* 5 vol.% and *c.* 20 vol.%, respectively, a short one at 930 °C/1000 MPa (BPQ-D41) and a long one at 920 °C/1.0 MPa (BPQ-D45). The reason for the higher melt fraction in the experiment at the lower temperature is because of the sluggish melting reactions, so insufficient time was available for melting to be completed in the short experiment. The yield strengths of these samples are 105 and 86 MPa, respectively (Fig. 4b). At these melt fractions, the samples deformed by a combination of melt-assisted granular flow and cataclastic flow. Melt-assisted granular flow is used to describe portions of the sample where many large, largely unfractured grains with rounded (reacted) edges, which are surrounded by melt on all sides, have flowed apparently en mass towards

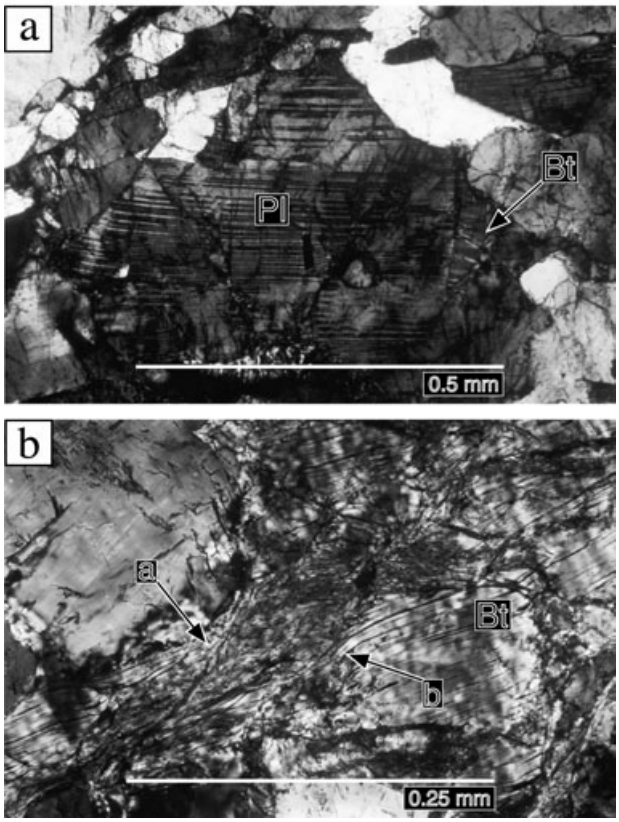

Fig. 6. Photomicrographs (crossed nichols) from experiment BPQ-D52 ($T=850$ °C). Three faults formed in this sample, with one major fault near the base of the sample.
(a) Fracturing of plagioclase grain along cleavage planes and a rare kinked biotite grain with {001} plane subparallel to σ_1.
(b) Close up of biotite in fault zone. Note that the biotite either fractures {a} with extreme disruption of the structure in a fault zone or {b} is rotated and shears along its {001} plane.

the edges of the sample. Cataclastic flow is used to describe regions of the samples which have intensely fractured angular grains, as in the 2 M samples, with grain sizes much smaller than the original grain size; they are surrounded by melt and have flowed in response to deformation. The difference in these two behaviours is that melt-assisted granular flow occurs when grains have been disaggregated from the framework of the sample by fine solid reaction products and melt formation, with subsequent migration along grain boundaries. Most grains are not significantly strained or fractured, i.e. there was little or no grain-size reduction. Cataclastic flow occurs when melt-assisted granular flow cannot accommodate strain at rates fast enough to alleviate local pore pressures and fracture is induced. The domains of mixed melt-assisted granular flow and cataclasis in both BPQ samples occur towards the bottom third of the cores. However, the grains in the mixed zone in BPQ-D41 (*c.* 5 vol.% melt fraction) are much finer grained and more angular than those of BPQ-D45 (*c.* 20 vol.% melt fraction). The grains in the sample from experiment BPQ-D45 have more rounded edges and are larger (Fig. 8c). There are few indicators of deformation in the upper portion of the sample from experiment BPQ-D45. Melt pockets with partially reacted biotite grains are common and edges of these pools are rounded. Melt is distributed along foliation, parallel to the main compression direction, and is directly associated with reacted biotite grains (Fig. 8d).

High melt fraction experiments

One high melt fraction 2 M experiment (2 M-D16) was conducted at 800 °C and 700 MPa generating a melt fraction is between 35 and 40 vol.%, but higher locally due to melt flow. The sample is weak and flow of melt within the sample is indicated by several observations. These include melt pools along the edge of the capsule and down below the edge of the lower spacer (a low pressure region produced during deformation); relic minerals that appear to have rotated within the melt and redistribution of muscovite-dehydration melting products; reaction products that are randomly oriented within pools of melt (glass); and relic quartz, feldspar and biotite grains which are largely undeformed, with few fractures in quartz and feldspar and no kinking in biotite grains (Fig. 9a). In this experiment, a pressure gradient developed and provided a driving force for melt to move to the low pressure region outside of the bottom spacer. These regions are now composed dominantly of melt (glass) with prismatic aluminosilicate and few relic grains of quartz and plagioclase (Fig. 9a).

The short BPQ experiment conducted at 950 °C/1000 MPa (BPQ-D32) contained a high enough melt fraction (*c.* 35 vol.%) for the sample to deform via macroscopically ductile flow, accommodated by flow of melt. Most biotite grains have reacted out from the sample, and only a few partially reacted grains remain at the top and base of the charge. Quartz and feldspar grains in this sample are unfractured and do not appear to be strained (Fig. 9b–d). Melt and reaction products have flowed to the outer edges of the sample during the experiment (Fig. 9c,d). The orientations of the relic quartz and feldspar grains, however, do not appear to be disturbed, even in the regions from which all biotite has reacted out and the grains are observed suspended in melt (glass) (Fig. 9b).

DISCUSSION

Interpretation of experiments

2 M experiments: The results of both of the sets of experiments performed show a drop in strength from subsolidus conditions to low melt fractions (Fig. 10a).

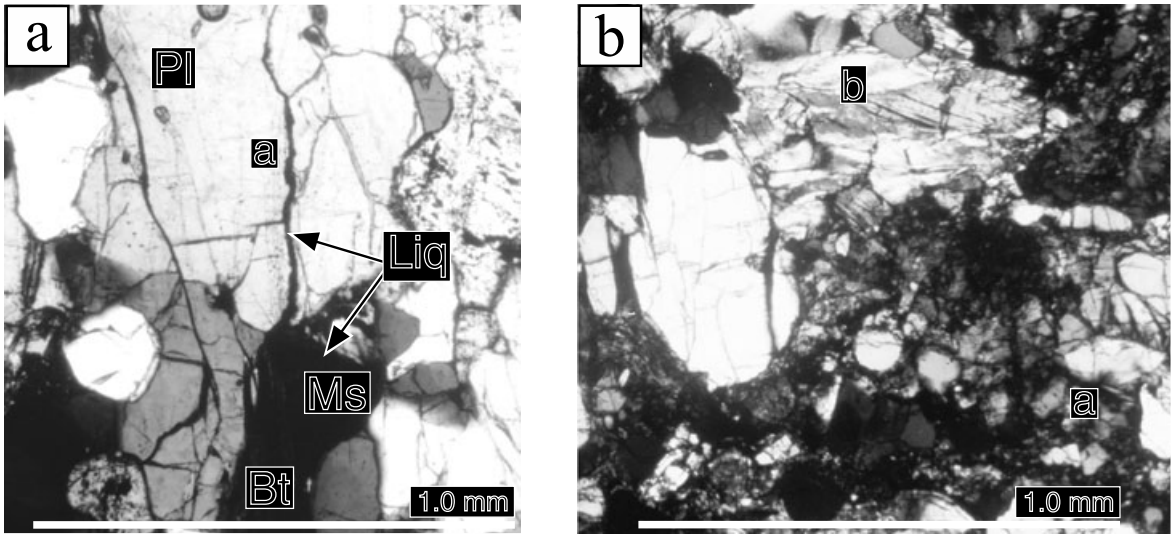

Fig. 7. Crossed nichols photomicrographs of examples of melt-induced fracturing and cataclastic behaviour in two samples; 2 M-D30 (a) and 2 M-D23 (b). (a) Vertical glass-filled fracture {a} through a plagioclase grain adjacent to a partially reacted muscovite grain and an unreacted biotite grain. (b) {a}Cataclastic zone in lower portion of sample, intermixed quartz, feldspar and melt. {b} is a partially reacted muscovite grain adjacent to the cataclastic zone with kinks and banding. Strain in this sample is accommodated by the development of pervasive cataclasis in the lower third of the sample and by moderate kinking of muscovite and biotite grains in the upper portion of the sample.

The magnitude of the initial drop in strength (as a percentage of the original subsolidus strength) is much larger and more immediate in the 2 M experiments (Fig. 10b).

All 2 M samples with melt present have approximately the same strength. This decrease in strength of 2 M samples with melt present occurred as a shift of deformation style from primarily kinking of mica to cataclastic flow is observed. The behaviour of the sample during the subsolidus experiment is primarily controlled by the orientation of the foliation in the sample, allowing the mica to accommodate strain by kinking, which is most intense adjacent to stronger and less deformed quartz and feldspar grains. At the onset of melting, large cataclastic regions developed in the samples, but outside these regions the samples were largely undeformed with only few fractures and some kinking of mica grains. From these results, we infer that without melt present, the accommodation of strain is distributed and accommodated by kinking of mica grains. However, in the presence of melt initiation of deformation induces cataclasis and strain is partitioned into discrete cataclastic zones. Where the melt fractions are the highest, strain is accommodated by the melt; quartz and feldspar grains are largely unfractured. This progression indicates that when muscovite-bearing assemblages begin to melt, what strength the rocks have is immediately lost via the development of cataclasis. We interpret these cataclastic zones as focused regions of high permeability.

The presence of cataclasis at low melt fractions is also interpreted to be due to the large dilational strain associated with the muscovite-dehydration melting reaction. The volume of melt produced at the solidus increases melt pore pressure. The pore pressure then lowers the effective stress necessary to induce fracturing (Davidson *et al.*, 1994). There is no obvious time dependence for the amount of melt present in short vs. long 2 m experiments, as there is in the gneiss experiments. This suggests that melt production is rapid, and moreover, significant melt fractions are produced at near solidus conditions. This probably occurs because of the lack of solid solution effects in muscovite as compared to biotite.

BPQ experiments: The results of the BPQ set of experiments also show a decrease in the strength of the samples with melt present (Fig. 10a). The strongest sample (no melt present) deformed in a purely brittle manner with strain accommodation accomplished partly by intragrain fracturing in quartz and feldspar and partly by kinking in suitably oriented biotite grains. However, the majority of strain was accommodated by the development of through-going faults. The early development of portions of these faults may involve biotite grains that fractured or slipped along basal planes in conjunction with the intergrain fracturing of quartz and feldspar. We interpret this as the reason for the decrease in strength observed in the differential stress vs. strain curve prior to the rapid loss of strength when the final development of through-going faults occurs.

At low melt fractions (1 vol.% or less), the strain is accommodated partially by fracture and the grain size reduction of quartz and feldspar grains, and flow

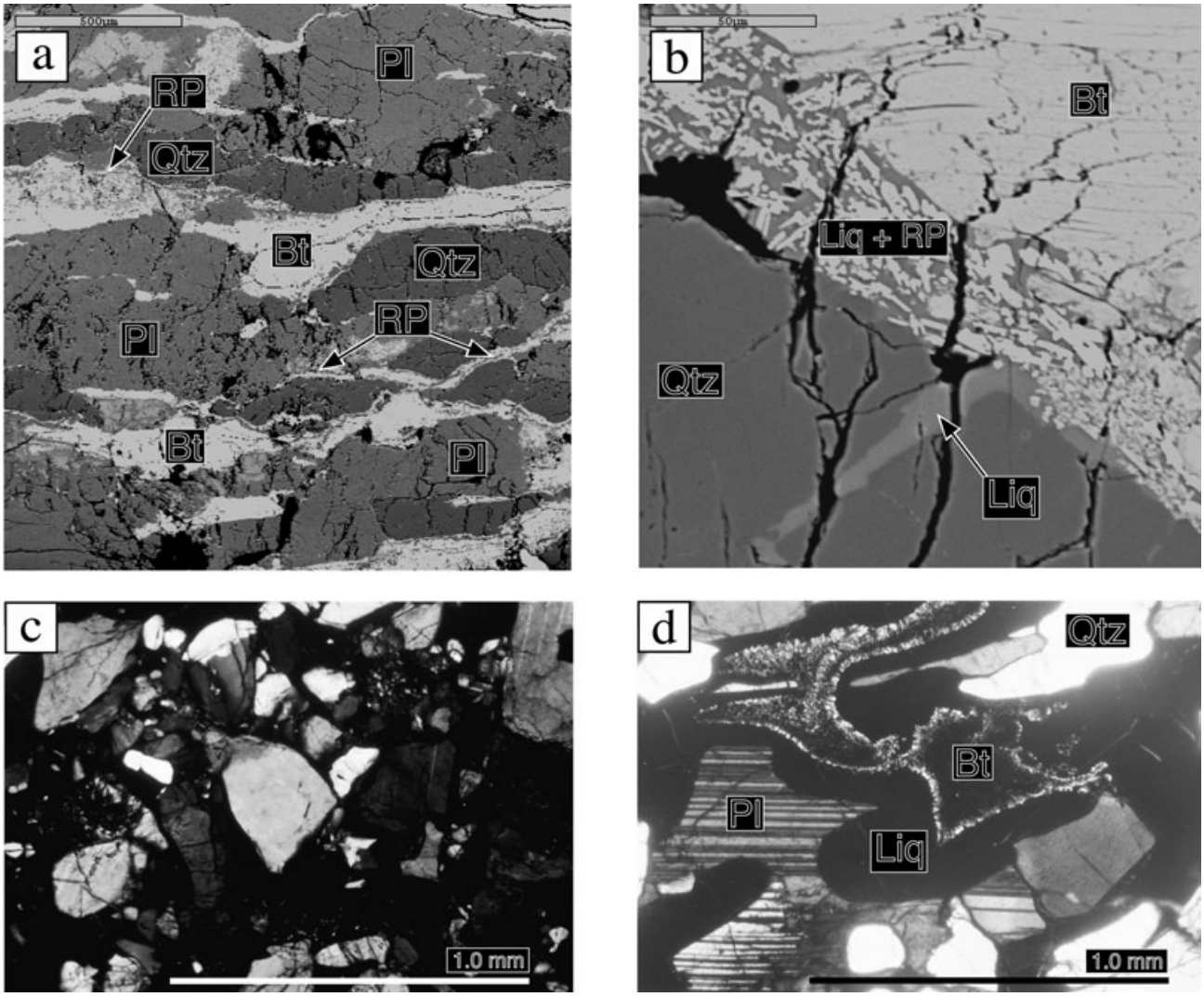

Fig. 8. SEM backscatter images and crossed-nichols photomicrographs showing the development of the melt-present behaviours of the BPQ samples. (a) BPQ-D38 ($T=900$ °C); the mica below the plagioclase grain are partially reacted, grain size has been reduced and the grains appear to have flowed about stronger quartz and feldspar grains. (b) BPQ-D40 D40 ($T=920$ °C), shows a close up of the boundary between a quartz grain and reacted biotite grain. Reaction products and melt line the boundary between the quartz and biotite grain with, in some cases, melt entering a fracture in the quartz grain. Large black cracks that go through melt and grains are from differential expansion of materials during unloading. (c) and (d) show examples of mixed behaviour in BPQ-D45 ($T=920$ °C). (c) Photomicrograph (cross nichols) of the mixed melt-assisted granular flow and cataclastic zone which developed in the lower portion of BPQ-D45. (d) Photomicrograph from the upper portion of the sample from experiment BPQ-D45. This is a good example of the microstructure of relatively unstrained regions. The strain is partitioned into the zones of melt-assisted granular flow and cataclasis, leaving these regions relatively undeformed. Note the scalloped edges of quartz and feldspar grains and remnant biotite grain in the middle of the melt.

of melt plus solid reaction products along foliation. These samples also have through-going fractures, but in the case of BPQ-D38 (900 °C, <1 vol.% melt), a smaller decrease in strength was observed than in experiment BPQ-D40 (920 °C, *c.* 1 vol.% melt, Fig. 10a,b). BPQ-D38 has a number of conjugate fractures which are lined with finely ground biotite, quartz and feldspar grains. In both samples, the partially reacted biotite grains and their reaction products have flowed to accommodate some of the strain, but the movement of material was unable to accommodate all of the strain, thus the development of the late, small faults.

When the melt fraction reached *c.* 5 vol.% (BPQ-D41), the strength decreased further and a second set of behaviours developed. There is melt flow along grain boundaries which disaggregates the framework of quartz and plagioclase grains and allows for melt-assisted granular flow. Locally, there is development of high melt pore pressures, causing cataclasis. These processes lead to a mixture of melt-assisted granular flow and cataclastic flow to accommodate deformation.

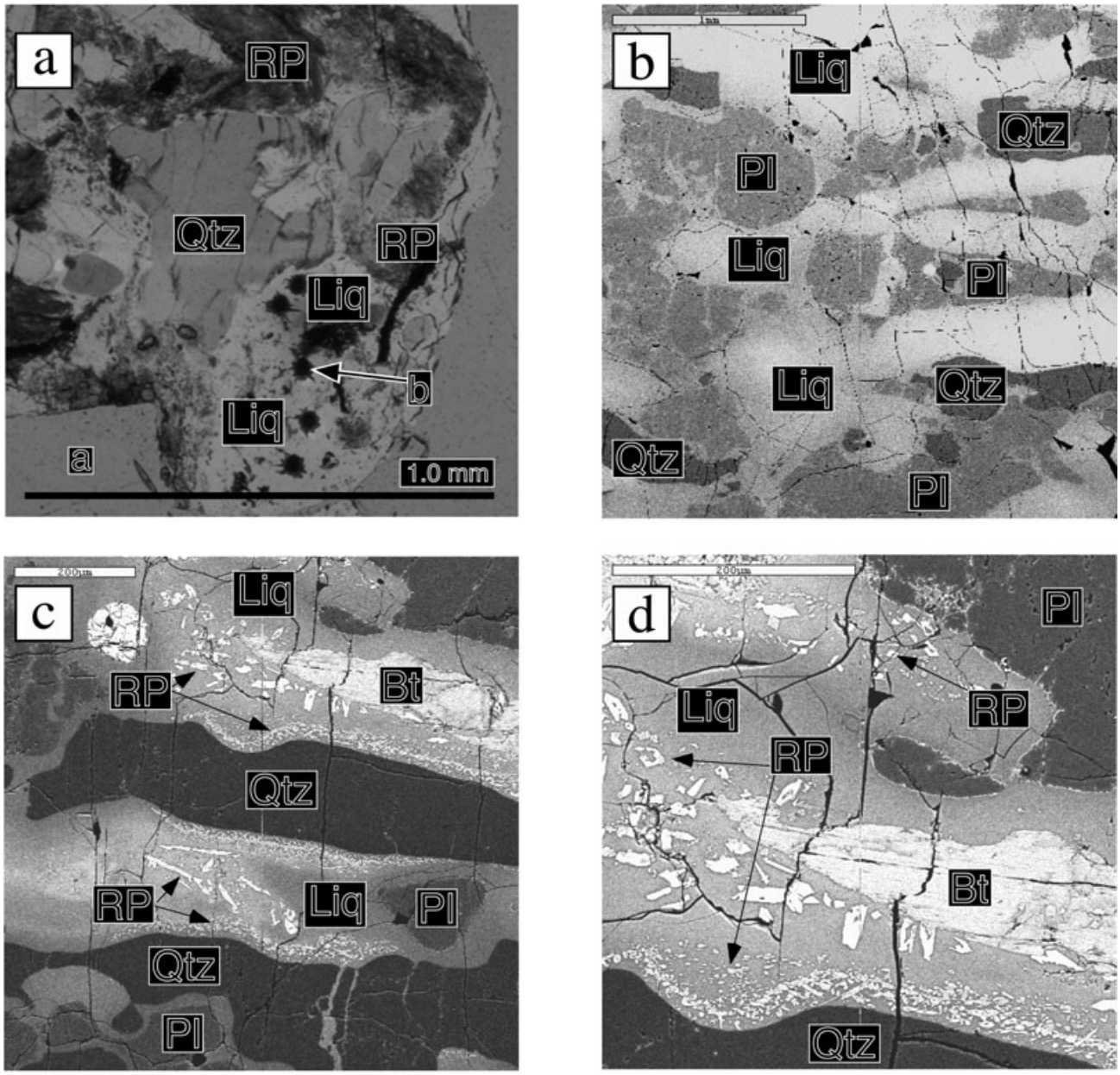

Fig. 9. Photomicrograph (a) and three SEM backscatter images show the behaviours of high melt fraction samples. (a) 2 M-D16 ($T = 800$ °C). This sample exhibits ductile flow due to the high melt percentage (up to 40% melt). The centre portion of the sample has undeformed quartz, feldspar and biotite grains which have been rotated due flow of melt within the sample. The portion of the sample shown is from the bottom right edge of the sample, where melt has been driven down the lower ZrO_2 piston by change in pressure gradient. The position of the piston is indicated by {a}. The 'bullet holes' present in the sample {b} are from Laser Ablation Inductively Coupled Plasma Mass Spectrometry (LA-ICPMS) analyses conducted on glass in this sample and are approximately 50 μm in diameter. (b) (c) and (d) SEM backscatter images of experiment BPQ-D32 ($T = 950$ °C). (b) This image was taken from the middle of the sample near the hot spot, all biotite has reacted out and melt has been squeezed toward the edge (right hand side of image) of the sample, leaving the remnant grains in the middle of the sample in their original orientations. (c) This image shows partially reacted biotite, reaction products (needle like opx + spinel grains) and melt. The quartz and feldspar grains have rounded edges and are relatively unfractured. Melt has flowed toward the outer edge of the sample along the foliation. Again, large black cracks that go through melt and grains are from differential expansion of materials during unloading. (d) close up of the upper central part of (c).

When compared to cataclastic zones observed in samples from the 2 M study with similar melt fractions, the zones of cataclasis in 2 M samples are sharply defined, grains are intensely fractured and the small grain size is uniform in these zones. In the mixed zones of the BPQ samples, there are large, largely unfractured grains that are surrounded by melt and some zones of grain size reduction (Fig. 11). The low melt fraction

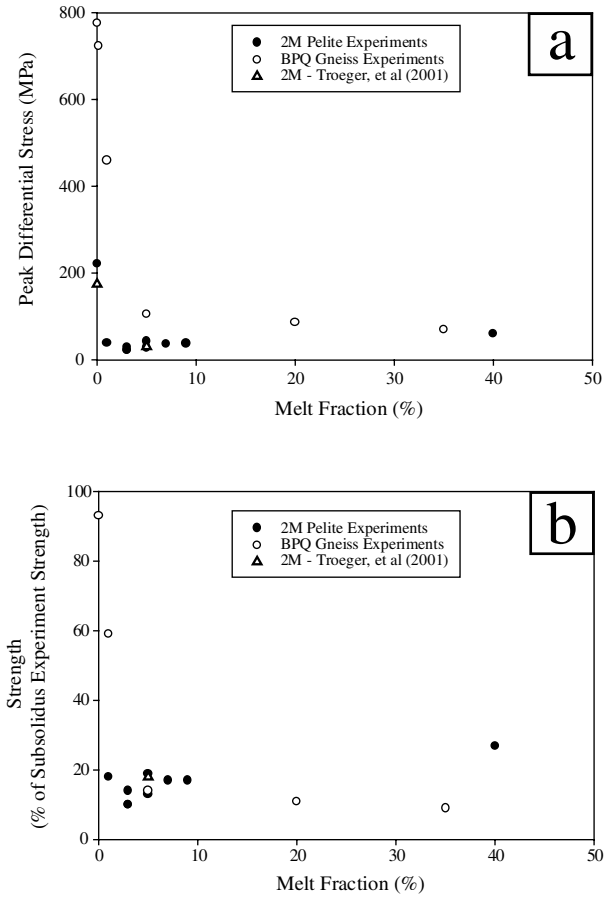

Fig. 10. (a) The peak differential stress vs. melt fraction data for all experiments. The differential stresses of the 2 M experiments show a large (*c.* 140 MPa) decrease from the subsolidus strength to samples with melt present. All melt-present 2 M samples have approximately the same strength within the resolution of load measurement in a solid media assembly used for this study. The decrease in strength in BPQ samples is not so abrupt; with low values obtained until higher melt fractions (5 vol.%). The strengths of these samples approach the strengths of 2 M samples as mixed melt-assisted granular flow and cataclasis begin to occur in the BPQ samples. 2 M data for deformation perpendicular to foliation orientation are plotted for comparison from Troeger *et al.* (2001) (see text for discussion). (b) This graph presents the same data but the peak strengths are plotted as a percent of subsolidus peak strength. The 2 M and BPQ samples are significantly different up to melt fractions of 5 vol.%, but thereafter show little difference at higher melt fractions. This indicates that there will be little difference in the strengths between the two rocks at crustal yield stresses at high melt fractions, which based on a power law decrease in strength as a function of strain rate.

samples (BPQ-D41 and BPQ-D45) switch from evenly mixed cataclasis and melt-assisted granular flow in the sample with a 5 vol.% melt fraction (BPQ-D41) to primarily melt-assisted granular flow with small zones of cataclasis in the sample with 20 vol.% melt (BPQ-D45). In both samples, strain is strongly partitioned into the zones of mixed behaviour. At high melt fractions (*c.* 35 vol.%), BPQ-D32 deformed by macroscopically ductile flow of melt and suspended relic grains along foliation, and accumulation of melt was observed at the edges of the capsule.

In the gneiss experiments there is a clear dependency of melt fraction with time of experiment. Melt fractions are higher for the 'long' experiments than the 'short' experiments, in contrast to the 2 M experiments. This suggests that biotite-dehydration melting, at least under experimental conditions, produces melt at a slower rate, perhaps due to solid-solution in the biotite, combined with the slow melting reaction kinetics. This also suggests that melt and product phases are being formed during deformation of the sample, especially during the short experiments.

We attribute the difference in melt-solid microstructure development at low melt fractions in the metapelite and gneiss to the contrasting behaviour of the two different dehydration-melting reactions. We suggest that the difference in dilational strain associated with melting can help to explain the difference in behaviour between the two rock types deforming in the presence of melt; a larger volume of melt is generated at the initiation of muscovite-dehydration melting in contrast to the biotite-dehydration melting reaction (Fig. 11). The biotite-dehydration melting reaction does not produce this immediate drop in strength by development of cataclasis. We propose that this is possibly due to the low dilational strain of this melting reaction (0.6%; Rushmer, 2001). At lower melt fractions, this will not produce enough pore pressure to induce fracturing, but may be enough to allow migration along grain boundaries. The melt, as seen for example in the experiment BPQ-D40 with 1 vol.% melt, has migrated along foliation, even at the high strain rates used in this study.

Comparison with previous experimental work

Previous experimental studies of deformation of single crystal muscovite and biotite samples under subsolidus conditions (Kronenberg *et al.*, 1990; Mares & Kronenberg, 1993) have found that strength and deformation mechanisms in mica are highly dependent on the orientation of the {001} cleavage plane relative to σ_1. In this experimental study, subsolidus samples experience a strain weakening at higher strains than observed in the single crystal studies, but are still stronger than samples with the {001} plane in the preferred shear orientation (45° to σ_1; Kronenberg *et al.*, 1990; Mares & Kronenberg, 1993). The mica in the 2 M sample deformed at subsolidus conditions exhibit similar kinking as observed by Mares & Kronenberg (1993) and Kronenberg *et al.* (1990). Quartz and feldspar grains however, enhance the development of kinks, due to the addition of larger local shear stresses at the interface between quartz/feldspar grains and mica grains.

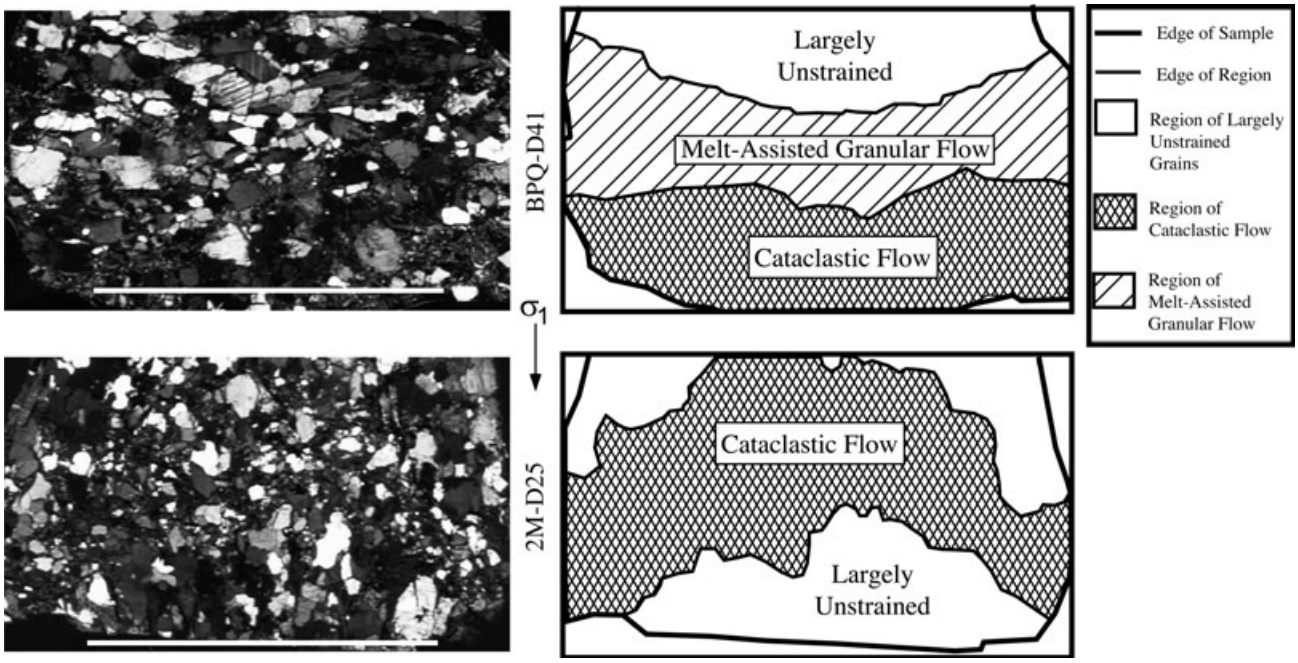

Fig. 11. Photomicrographs to contrast examples of mixed melt-assisted granular flow and cataclasis (BPQ) and purely cataclasis (2 M) in the two samples, deformed at the same bulk strain rate and with the same melt fraction (5 vol.%). Both photomicrographs are taken in crossed nichols and scale bars are 5 mm. Both of these experiments were conducted close to the solidus of the hydrous phase-dehydration melting reaction of each respective assemblage. The upper photomicrograph and deformation behaviour region map show mixed behaviour (melt-assisted granular flow and cataclasis) that developed during experiment BPQ-D41 (upper photomicrograph, $T = 930$ °C) The upper photomicrograph and map are from the lower third of BPQ-D41. The two zones of differing behaviour are apparent when the grain size is compared between the two. The region of dominant melt-assisted granular flow in BPQ has grains which are partially reacted, few fractures and melt has flowed along grain boundaries, disaggregating those grains. The region of cataclasis has intense grain fracturing. The cataclastic zone which developed in 2 M-D25 (lower photomicrograph, $T = 740$ °C) has no larger grains which are present in the cataclastic zone and the zone of cataclasis is extensive.

Other experimental studies on mica-bearing quartz feldspar aggregates at subsolidus conditions, both natural and synthetic (Shea & Kronenberg, 1993 and Tullis & Wenk, 1994, respectively), have shown that the strength of the sample is dependent on the percentage of mica (the weakest phase) present. The percentage of mica necessary to change from a strong quartz/feldspar framework aggregate to a weak mica framework aggregate was somewhat different in the two studies, <25 vol.% (Shea & Kronenberg, 1993) or <15 vol.% (Tullis & Wenk, 1994), respectively. As the percentage of mica present in both of the starting materials used in this study is *c.* 30 vol.%, the behaviour should not be dominated by the deformation of quartz and/or feldspar, but by the micas. The orientation of foliation in the two starting materials should therefore have a large control over the strength of the sample. The BPQ subsolidus experiment was about three times stronger than the corresponding 2 M experiment. This was first attributed only to the differences in foliation orientation of the two starting materials. To test this attribution, subsolidus experiment was conducted by Troeger *et al.* (2001) on the 2 M starting material. The results show that the strength of the 2 M sample under the same conditions, but with the foliation perpendicular to σ_1, had a similar strength to the 2 M sample with foliation parallel to σ_1 (Fig. 10a,b). The 2 M rock may therefore be isotropic in as far as the relation between foliation orientation and strength are concerned, at the strain rates of the experiments. This could be due to the presence of quartz and feldspar in combination with the variations in mica orientation in the sample, e.g. not all mica grains were perpendicular or parallel to σ_1. The natural variation of the mica orientation in the starting material in addition to heterogeneous distribution of quartz and feldspar in relation to mica may play a more important role in controlling overall yield strength of the natural material rather than mica orientation and/or the ratio of mica to quartz plus feldspar individually.

The immediate development of melt-enhanced embrittlement in the 2 M samples is most likely due to the rapid increase in pore pressure, as discussed above. Also, this affect does not appear to be foliation orientation dependent. An additional experiment conducted by Troeger *et al.* (2001) at the same T–P–$\dot{\varepsilon}$ conditions as 2 M-D23 ($T = 740$ °C, $P_c = 700$ MPa,

$\dot{\varepsilon}=1\times10^{-5}$ s^{-1}), but with the foliation perpendicular to σ_1, deformed via cataclastic flow and is as weak as the foliation parallel experiment (Fig. 10a,b). Although relic grain shapes seem to reflect foliation orientation, the results suggest that during deformation in the presence of melt in the 2 M metapelite, the effects of foliation orientation in the laboratory are not significant in terms of rock strength and the development of melt-present deformation microstructures. The strength of samples is similar because deformation is accommodated in both experiments by cataclastic flow.

The behaviour of both the 2 M samples and BPQ samples differs in some ways from previous experimental studies of natural rocks undergoing dehydration melting during deformation. In the deformation study by Rutter & Neumann (1995), the muscovite and biotite-bearing Westerly granite developed melt lined fractures and dilatant shear zones at the lowest melt fractions ($P_c=250$ MPa, $T=800$–1100 °C, $\dot{\varepsilon}=1\times10^{-5}$ s^{-1}). The mode of muscovite in the Westerly granite is small (*c.* 5 vol.%) which may explain the difference in behaviour. At higher melt fractions (5–15 vol.%), cataclastic shear zones developed in the Westerly granite cores. BPQ samples also develop cataclasis between 5 and 15 vol.% melt, but the cataclasis observed in BPQ samples is mixed with zones of earlier formed melt-lined grain boundaries parallel to foliation. The proportion of cataclasis also decreases as the melt fraction increases. A better comparison of BPQ is with another lower-crustal assemblage which is stable at similar conditions as the biotite gneiss. Such a study (Rushmer, 1991, 1995) investigated deformation and partial melting in a natural amphibolite ($P_c=800$ and 1800 MPa, $T=650$ °C – 1100 °C, $\dot{\varepsilon}=1\times10^{-5}$ s^{-1}). The BPQ strength behaviour is most similar to that of amphibolite deformed at 800 MPa at the same strain rate. Strength under subsolidus conditions ranges from 1060 to 930 MPa then falls to 120 MPa between 15 and 20 vol.% melt. Through-going faults dominate the deformation style between 5 and 10 vol.% melt, then the amphibolite becomes disaggregated at 15–20 vol.% melt. Extensive cataclasis is not observed at the lower melt fractions.

Dell'Angelo & Tullis (1988) also deformed a partially melted natural aplite (water-saturated, 10–15 vol.% melt, $T=900$ °C, $P_c=1500$ MPa) that developed cataclastic zones when deformed at $\dot{\varepsilon}=1\times10^{-5}$ s^{-1}. When deformed at a lower strain rate ($\dot{\varepsilon}=1\times10^{-6}$ s^{-1}) the samples did not develop cataclastic zones at low melt fractions (5–10 vol.%). Melt could migrate along grain boundaries, which was sufficient to relieve pore fluid pressure. At 15 vol.% melt, however, the sample developed cataclasis. This was attributed to the melt not being able to migrate along grain boundaries at rates sufficient to relieve the melt pore pressure. As the ΔV of water-saturated melting is negative (based on the slope of the wet melting curve in P–T space) there will be effectively no dilational strain imparted on the rock by wet melting alone. The behaviour of biotite-bearing assemblages, and possibly amphibolites, undergoing dehydration-melting at lower crustal conditions during deformation at lower strain rates than used in this study, may be more similar to that observed by Dell'Angelo & Tullis (1988).

The combination of these results suggests that there may be significant rheological differences in the behaviour of muscovite-bearing assemblages (i.e. middle crust assemblages) and biotite-only, and perhaps amphibole-only bearing assemblages (i.e. lower-crustal assemblages) undergoing dehydration melting during deformation. To compare the behaviour of these different assemblages the log effective viscosities were calculated and plotted against melt fraction for both the 2 M and BPQ experiments (Fig. 12). The log effective viscosities of the 2 M experiments are lower than those of the BPQ experiments until high melt fractions (ductile flow) are achieved. The production of focused permeability concomitant with low melt fractions suggests that rapid melt segregation accompanied by transient fracturing of the middle crust is a possibility during deformation and melting of muscovite-bearing pelite. Alternatively, if melt does not leave its source due to local, or outcrop scale, confinement of the melt pathways, melt-rich weak regions can be generated easily in the middle crust. It suggests also that lower-crustal rheologies may be affected by allowing melt to remain along grain boundaries until higher melt fractions are achieved (hence longer residence times between melt and source). The lower crust may weaken, but not transiently, as in the middle crust. The differences in the behaviours may be attributed to the differences in melt production, dilational strain associated with partial melting and confining pressures.

The lower confining pressure may also decrease the strength of the muscovite-bearing assemblages. To further investigate this idea, the log effective viscosities of the experimental deformation studies of partially molten natural rocks being deformed at $\dot{\varepsilon}\sim1\times10^{-5}$ s^{-1} discussed above are compared. In Fig. 12, there is a separation between the middle crustal assemblages and lower crustal assemblages. The effects of higher pressure on effective viscosity (which should increase with increasing confining pressure) are part of the reason for the separation, but the effective viscosity of an amphibolite undergoing dehydration melting at $P_c=800$ MPa, 20 vol.% melt fraction (Rushmer, 1991) is still higher than that observed for the 2 M samples undergoing dehydration melting at 700 MPa. The effective viscosity, however, of this sample is almost exactly that of the BPQ sample at the same melt fraction and a higher confining pressure (1000 MPa).

The middle crustal assemblages have lower effective viscosities up to 25 vol.% melt than the lower crustal assemblages, but there is little data at higher melt

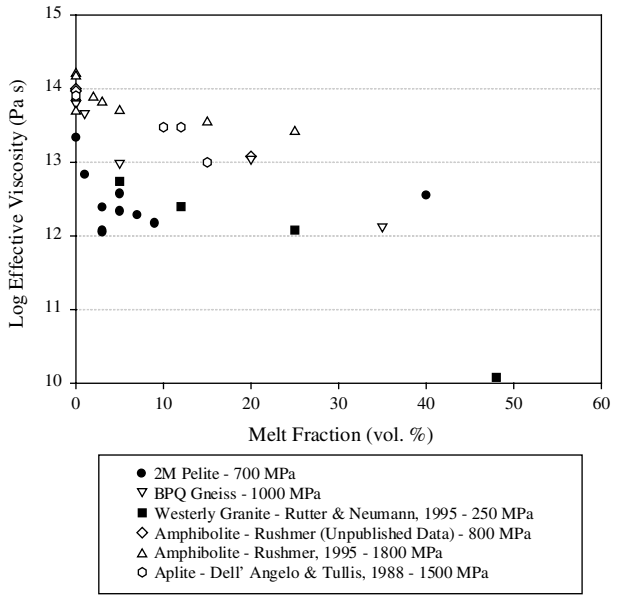

Fig. 12. Log effective viscosity vs. melt fraction with samples from this study and for other experimental studies using natural starting materials and strain rate of 1×10^{-5} s^{-1}. All of the data presented above are from studies of partially molten natural rocks (all fluid-absent dehydration melting of hydrous phases except for Dell'Angelo & Tullis, 1988 who added water to produce melt). All data are calculated from peak strength values and published strain rates. The studies are labelled by authors and the confining pressure at which the experiments were performed. The data are divided into two sets; lower crustal assemblages (open symbols) [biotite ($P_c=1000$ MPa) and amphibole ($P_c=800$ and 1800 MPa) dehydration melting or water saturated melting ($P_c=1500$ MPa)] and mid to upper crustal assemblages (filled symbols) [muscovite-dehydration melting ($P_c=250$ and 700 MPa)].

fractions as these strength data are probably too high due to friction in the solid-media apparatus. The effective viscosity of the Westerly Granite experiments conducted by Rutter & Neumann (1995) may be comparable to the effective viscosities of the 2 M samples, although at much lower confining pressures. This holds up to the highest melt fractions where the resolution of measurement of load of the solid media assembly used in this study limits the ability to measure accurately the low strength of samples and therefore to calculate the effective viscosity of those samples. It is expected that if it was possible to measure very low strengths in the solid media assembly, the strength of the high melt fraction samples would be very low as the strength of the high melt samples is controlled by the melt (Rutter, 1997).

The lower crustal assemblages (biotite/amphibole dehydration melting studies and water saturated melting study) have higher effective viscosities. The effective viscosities all decrease in a similar manner up to 25 vol.% melt fraction. This indicates that the lower crustal rocks may not be as weak as the mid crustal rocks until the behaviour of the rocks is controlled by the presence of large quantities of melt. One exception, and likely possibility, is that melt-filled grain boundaries can induce grain boundary diffusion deformation mechanisms and weakening would be achieved in this manner.

The development of pathways for melt migration on the grain scale is the first step toward migration of melt from the source. A series of schematic drawings are shown in Fig. 13(a)–(e), which shows the development of the pathways produced during muscovite-dehydration melting under deformation. Figure 14a,b shows the development of pathways during biotite-dehydration melting. These two series of drawings are based on the results of this study and present what is expected to happen on the grain scale in natural systems. The muscovite-dehydration melting model has five steps, four of which should occur in rapid succession after the onset of melting. The five steps are: (1) prior to melting (Fig. 13a); (2) the onset of melting and fracturing (Fig. 13b); (3) the development of melt-enhanced embrittlement (Fig. 3c); (4) melt is driven out of these zones due to the development of pressure gradients (Fig. 13d); and (5) the remaining zones heal forming the now melt-depleted rock (Fig. 13e). Melts formed from muscovite dehydration-melting in metapelites are suggested to migrate from the zone of reaction at low melt fractions through an interconnected network of cataclastic zones and melt-induced fractures, steps 1–3. This network, which forms at low melt fractions in muscovite-bearing assemblages possibly plays a role in the formation of leucosomes and leucogranitic plutonic bodies, whose compositions reflect magma formed by muscovite-dehydration melting (Le Fort *et al.*, 1987; Watt *et al.*, 1996; Patiño-Douce & Harris, 1998). The development of pressure gradients in the protolith of muscovite-bearing assemblages will transiently enhance low (1–5 vol.%) melt fraction segregation along a fracture network. As melt fraction increases, the protolith is disaggregated by grain boundary melt migration and pressure will be more evenly distributed through the protolith and local pressure gradients may not drive the melt segregation process as effectively locally and buoyancy takes over. This could entrain many more residual solid grains in the magmas which are then transported and emplaced in the upper crust.

The biotite-dehydration melting model has two main stages (Fig. 14a,b). These steps can be repeated as the biotite continuously reacts, creating melt and reaction products and leaving a more chemically stable biotite. The small fractions of melt will be transported from the immediate source by migration along the foliation to sites of ponding. This process could occur many times if higher temperatures are reached in the lower crust and the relic biotite grains continue to react with plagioclase and quartz. If there is no region for significant ponding to occur then the region will not be drained (Sawyer, 1994), allowing for melt fractions to

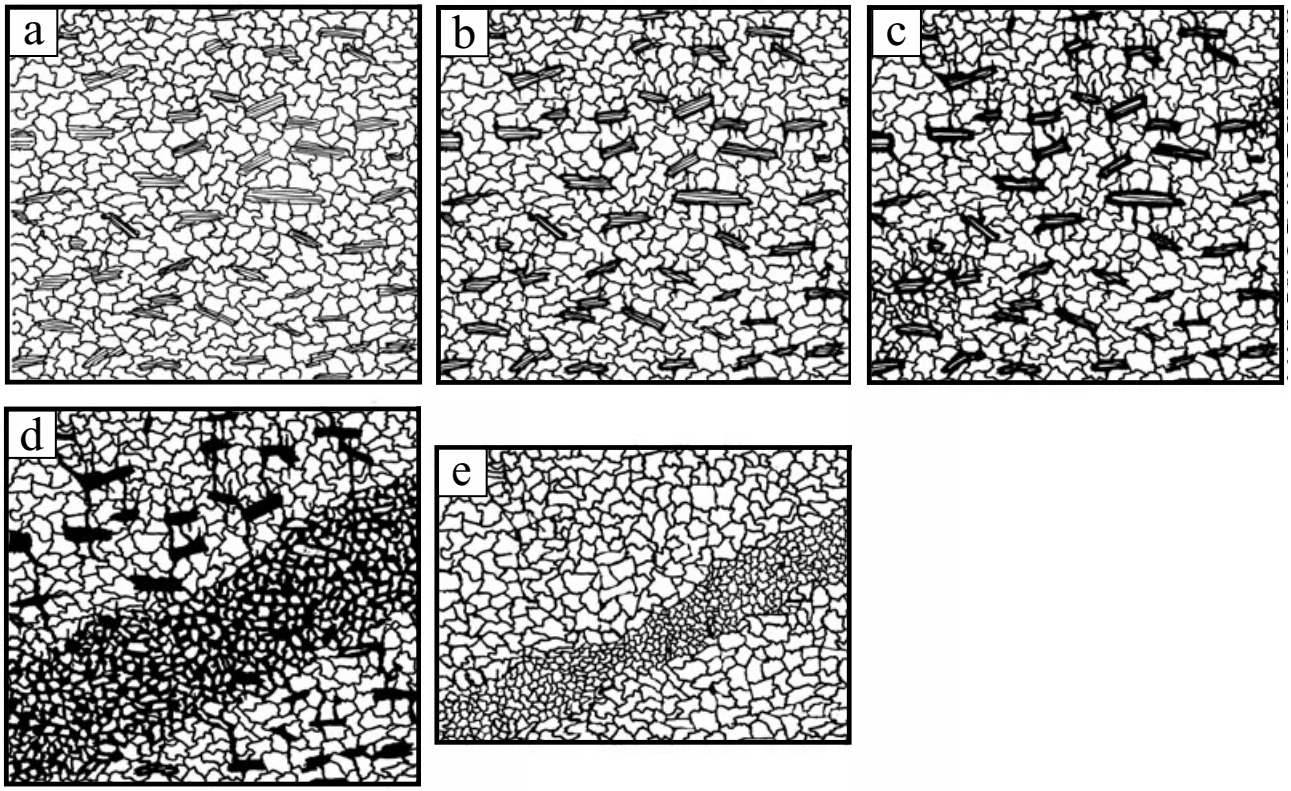

Fig. 13. This figure presents a series of schematic drawings showing the microstructure development during dehydration-melting in a muscovite-bearing assemblage. In all sketches σ_1 is oriented perpendicular to foliation defined by mica; compression direction top to bottom. Melt is shown in black. (a) shows a muscovite-bearing rock before the initiation of partial melting. (b) As muscovite-dehydration melting begins under deformation, the outer rims of muscovite grains begin to react with surrounding quartz and plagioclase grains. Small melt-filled cracks, oriented parallel to σ_1 begin to develop. Permeability is produced through a combination of cracking by reaction and melt pore pressure induced cataclasis. (c) Melt fraction increases (5 vol.% melt) and cataclastic zones begin to develop about pools of muscovite melt. This is due to the inability of melt to migrate from these zones at rates sufficient to relieve melt pore pressure. (d) Cataclastic zone is composed of highly fractured quartz and feldspar grains, reaction products (alumino-silicate, K-feldspar and biotite) and melt. Strain is now partitioned into the melt-rich zone and, if present, pressure gradients can drive melt segregation from the cataclastic zone at this stage. (e) The final stage shows the healed cataclastic zone with a finer grain size. Some small pools of melt (now crystallized) may remain ($\ll$1 vol.%). Very small melt fractions and some reaction products will likely be trapped in the host rock as the permeability of the rock decreases with healing of melt fractures outside of the cataclastic zone, eliminating interconnectivity (see also Sawyer, 2001).

increase in the zones of reaction to the levels which may cause disaggregation of the protolith, similar to the BPQ samples with 5–20 vol.% melt.

Possible mechanisms of magma segregation and transport in different crustal protoliths

The geological implications of the differences between the crustal dehydration-melting reactions are two-fold. First, melt generation and segregation in muscovite-bearing assemblages will be such that low melt volumes ($<$10 vol.%) may escape readily as the interconnected network needed for melt segregation can be generated at the onset of melting. Although leucogranites can be the result of fractionation processes (e.g. Scaillet *et al.*, 1990), some naturally occurring leucogranites can be compared with low fraction experimental melts derived from muscovite-dehydration melting reactions (Patiño-Douce & Harris, 1998). It is perhaps not coincidental that the muscovite-derived peraluminous Himalayan leucogranites investigated by Inger & Harris (1991), Ayers & Harris (1996) and Patiño-Douce & Harris, 1998) are low melt fraction granites with evidence of rapid extraction rates from their source. Melt residence times have been calculated by Ayers *et al.* (1997) for High Himalayan leucogranites, and their results, based on calculated temperatures of melt formation between zircon and monazite thermometry, indicate that the Himalayan leucogranites have had short residence times (i.e. melt in contact with the protolith), of 7–50 ka. The production of an interconnected network during partial melting of a muscovite-bearing metapelite, perhaps aided by Himalayan tectonics, may be a mechanism by which these low fraction melts

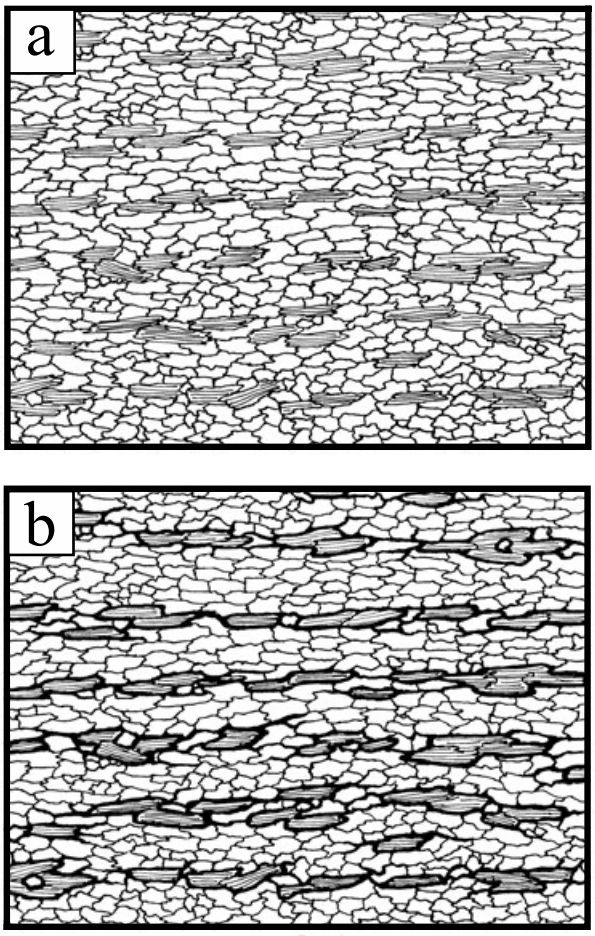

Fig. 14. These schematic drawings present the development of melt-interconnectivity in a biotite–quartz–plagioclase-bearing gneiss. As above, σ_1 is oriented perpendicular to foliation defined by mica; compression direction top to bottom. Melt is shown in black. (a) Rock with no melt present and a foliation normal to σ_1. (b) As the biotite begins to react with adjacent plagioclase and quartz grains, melt and reaction products (orthopyroxene, spinel and K-feldspar) form along grain boundaries which are controlled by the foliation orientation. Ideally, the melt will begin to migrate along grain boundaries to relieve pore pressure and strain is partitioned into the melt and the biotite grains which remain. It is most likely that during melt segregation small volumes of melt may remain in the source area or be slowly removed by flow along the foliation to low pressure areas, such as shear zones (e.g. Sawyer, 2001).

segregated. In lower crustal biotite-bearing assemblages, melt moves along grain boundaries releasing pore pressure and melt pathways are more controlled by pre-existing anisotropy in the rock (Sawyer, 2001). Unless pore pressure can be built up locally, melt-induced fractures may not be as easily formed.

Second, these differences in melt generation rates and residence times can have a profound effect on crustal rheology. Rheological profiles through time in orogenic belts are continuously being modified as the belt grows particularly if partial melting occurs, which is one of the most powerful ways to weaken rocks. The rheology of the middle and lower crust may alternatively be weak or strong, depending on rates at which melt is generated and segregated. Potentially, decoupling is possible in orogens with a melt-rich middle crust (Nyman *et al.*, 1995; Vanderhaege & Teyssier, 1997).

The production of high permeability zones during muscovite dehydration-melting may also have important consequences in regard to geochemistry. If muscovite-derived melts segregate early and efficiently along the earliest formed fracture network, major element composition will mirror muscovite-derived melt major element compositions but trace element abundance may be low with more erratic REE patterns, due to lack of dissolution of common accessory phases, such as apatite and monazite, which control REE behaviour (Watson *et al.*, 1996; Watt *et al.*, 1996; Harris *et al.*, 2000). However, cataclasis can also offer an environment where melt can obtain full geochemical equilibrium because of the reduction of grain size and increase of surface area within these zones which enhances reaction; perhaps also aiding in residual phase entrainment (Sawyer, 1998). In this scenario, magma needs to remain in the cataclastic, highly permeable zone so chemical communication between different sites of melting and accessory phases can be obtained. Both scenarios may occur during a single tectonic event; producing melts with different geochemical signatures.

Muscovite dehydration-melting may also produce magmas likely be transported quickly via mechanisms detailed by Clemens & Mawer (1992) and Petford *et al.*, 2000); rapid transport through dykes induced by positive volume change upon melting. It is unlikely that the biotite-dehydration derived magmas will be transported via this model of dyking (see Sawyer *et al.*, 1999 for alternative dyking scenarios) unless some ponding occurs allowing for significant melt volumes to be present to increase pore pressure and induce melt-enhanced embrittlement. It is more likely that biotite-dehydration derived magmas will flow along anisotropies in the protolith until focused zones of low pressures, such as shear zones, develop. Shear zone development, as a mode of magma transport, may be enhanced by the presence of melt itself (Brown & Rushmer, 1997). The process of melt moving out of the protolith will establish local pressure gradients allowing melt to flow toward the low pressure sites, i.e. shear zones. The rate at which melt can flow to these shear zones will be limited by the nature of the grain scale melt migration mechanisms. The control of melt migration on the grain scale by source anisotropy and the continuous rate of melt production by biotite-dehydration melting may cause this process to occur over long periods of time, forming multiple batches of melt which will flow from the protolith toward the shear zones. This is a mechanism for segregation of

melt at low melt fractions from the protolith and the feedback between the creation of shear zones and melt migration into these zones over longer periods of time will be efficient for extraction and transport of magma from the source. However, as magma moves to ponds at different levels in the crust, the mechanisms of melt transport will depend on a variety of local conditions, such as state of stress and temperature. Initial geochemical signatures from the source present in the magma will be modified by transport processes which allow ponding at different stages.

Application to natural settings

Two examples of melt-enhanced embrittlement in lower crustal assemblages have been observed in field based studies, both on the grain-scale (Watt *et al.*, 2000) and on the outcrop-scale (Davidson *et al.*, 1994). Watt *et al.* (2000) observed small networks of healed cracks in relic quartz grains that are found in K-feldspar and garnet grains in migmatites. The healed cracks are observed under cathodoluminescence imaging in an SEM and have the appearance of bright veins within the quartz grains. Subgrain boundaries, when viewed using the same technique, do not luminesce as brightly, so Watt *et al.* (2000) suggested they are due to healing of melt cracks formed by biotite-dehydration melting. In one sample of this study, melt-filled fractures are observed in a quartz grain located adjacent to a biotite reaction zone (Fig. 6c). These sorts of fractures are not observed in the quartz/feldspar grains in the limited cataclastic zones in samples from this study with low melt fractions (*c.* 5 or *c.* 20 vol.%). If the bright vein networks observed by Watt *et al.* (2000) are healed fractures previously filled with melt, they may represent local melt-enhanced embrittlement rather than reaction-induced fracturing *per se*.

Evidence of melt-enhanced embrittlement has been observed in outcrop scale. Davidson *et al.* (1994) observed conjugate sets of fractures filled with leucocratic material (melt) in amphibole-bearing migmatite gneisses in British Columbia, Canada. In one case the transition from ductile shearing to semibrittle fracture to completely brittle fracture is preserved in the outcrop. Davidson *et al.* (1994) attributed this transition to the development of pore pressure due to partial melting, which decreased the effective stress and induced fracturing. This behaviour may occur in regions of low melt fraction, with poor connectivity and high natural strain rates.

Partial melting in the lower crust is discussed by Sawyer *et al.* (1999) who studied consequences of biotite-dehydration melting in the Wuluma Hills, central Australia. Here partial melt is inferred to have migrated within the zone of reaction in response to changes in local pressure gradients due to anisotropies in the protolith. This process formed multiple generations of cross-cutting leucosomes of different compositions. This occurred because some melt remained in the source, but melt was lost in other zones that retained product feldspar and relic quartz. Therefore, these leucosomes reflect different stages of melt segregation efficiency or degrees of contamination. This process, which suggests protracted extraction of melt with melt migration paths controlled by structural anisotropies in the source, may reflect the nature of the biotite dehydration-melting reaction itself combined with deformation at slower strain rates.

CONCLUSIONS

Muscovite-dehydration melting during deformation in the laboratory causes the development of intense focused highly permeable cataclastic zones in samples with low melt fractions. There is a clear drop in strength from the subsolidus samples to the samples with low melt fractions (*c.* 1–*c.* 10 vol.%). At high melt fractions (40 vol.%) samples deform by ductile flow of melt containing undeformed relic quartz and feldspar grains. The development of cataclastic zones in conjunction with melt cracks will form an interconnected network of flow paths from which melt can be removed from the host rock. This will allow for segregation of melt from the host rock at low melt fractions. Whether full geochemical equilibration will occur, with or without entrainment of residual material, may depend on the presence of early melt-induced fractures and/or far-field stresses which can produce pressure gradients necessary to drive melt segregation at low melt fractions. This can also be true for other hydrous phases undergoing dehydration melting during regional deformation (i.e. in biotite- and hornblende-bearing rocks, Barbey *et al.*, 1989; Sawyer, 1991).

The experimental deformation behaviour of rocks undergoing biotite-dehydration melting during deformation contrasts with the behaviour of rocks undergoing muscovite-dehydration melting. In experiments conducted for this study, biotite-dehydration derived melts are observed to migrate along grain boundaries, dissagregating grains. Cataclastic behaviour is also observed in samples with melt fractions of 5 to 20 vol.% in combination with melt-assisted granular flow. When applied to natural settings, this melting process suggests protracted, continual draining of biotite-derived magma (with or without full geochemical equilibration) from the lower crust with melt migration paths controlled by structural anisotropies at the source, unless locally high melt pore pressure can develop.

ACKNOWLEDGEMENTS

CH and TR thank NSF support EAR-9706548. We also acknowledge many helpful discussions with

J. Pinkston, G. Gleason, J. Tullis, J. Ross, R. Stanley and K. Klepeis. D. Rubie generously supplied the 2 M pelite starting material. CH thanks the UVM Department of Geology for GTF support during this study, and A. McKinney, L. Troeger, G. DiToro and D. Goldsby. TR acknowledges helpful field discussions with R. Stanley, E. Sawyer, M. Brown, and K. Klepeis. Thorough and thought provoking reviews by E. Sawyer, D. Pattison and G. Gleason considerably improved the paper and are greatly appreciated.

REFERENCES

Ayers, M., Harris, N. & Vance, D., 1997. Possible constraints on anatectic melt residence times from accessory mineral dissolution rates: an example from Himalayan leucogranites. *Mineralogical Magazine*, **61,** 29–36.

Barbey, P., Bertrand, J.-M., Angoua, S. & Dautel, D., 1989. Petrology and U/Pb geochronology of the Telohat migmatites, Aleskod, central Hoggar, Algeria. *Contributions to Mineralogy and Petrology*, **101,** 207–219.

Barbey, P., Brouand, M., Le Fort, P. & Pecher, A., 1996. Granite-migmatite genetic-link: example from the Manaslu granite and the Tibetan slab migmatites in central Nepal. *Lithos*, **38,** 63–79.

Barbey, P., Macaudierre, J. & Nzenti, J. P., 1990. High-pressure dehydration melting of metapelites: evidence from the migmatites of Yalunde (Cameroon). *Journal of Petrology*, **31,** 401–427.

Brown, M. A., Brown, M., Carlson, W. D. & Denison, C., 1999. Topology of syntectonic melt-flow networks in the deep crust: inferences from three-dimensional images of leucosome geometry in migmatites. *American Mineralogist*, **84,** 1793–1818.

Brown, M. & Rushmer, T., 1997. The role of deformation in the movement of granitic melt: views from the laboratory and the field. In: *Deformation-Enhanced Melt Segregation and Metamorphic Fluid Transport* (ed. Holness, M.), pp. 111–144. Chapman & Hall, London.

Brown, M. & Solar, G., 1998. Shear-zone systems and melts: feedback relations and self-organization in orogenic belts. *Journal of Structural Geology*, **20,** 211–227.

Clemens, J. & Mawer, C., 1992. Granitic magma transport by fracture propagation. *Tectonophysics*, **204,** 339–360.

Connolly, J., Holness, M., Rubie, D. & Rushmer, T., 1997. Reaction-induced microcracking: an experimental investigation of a mechanism for enhancing anatectic melt extraction. *Geology*, **25,** 591–594.

Davidson, C., Schmid, S. & Hollister, L., 1994. Role of melt during deformation in the deep crust. *Terra Nova*, **6,** 133–142.

Dell'Angelo, L. & Tullis, J., 1988. Experimental deformation of partially melted granitic aggregates. *Journal of Metamorphic Geology*, **6,** 495–516.

Gardien, V., Thompson, A. B., Grujic, D. & Ulmer, P., 1995. Experimental melting of biotite + plagioclase + quartz +/− muscovite assemblages and implications for crustal melting. *Journal of Geophysical Research*, **100,** 15581–15591.

Gleason, G., Bruce, V. & Green, H. W., 1999. Experimental investigation of melt topology in partially molten quartzofeldspathic aggregates under hydrostatic and non-hydrostatic stress. *Journal of Metamorphic Geology*, **17,** 705–722.

Harris, N. B. W., Inger, S. & Hawkesworth, C. J., 1991. Crustal evolution during intercontinent collisions in the Himalayas and southern Tibet. In: *Sixth meeting of the European Union of Geosciences* (ed. Anonymous) Terra Abstracts, Blackwell Scientific Publications, Oxford.

Harris, N. B. W., Vance, D. & Ayres, M. W., 2000. From sediment to granite: timescales of anatexis in the upper crust. *Chemical Geology*, **162,** 155–167.

Hartel, T. H. D. & Pattison, D. R. M., 1996. Genesis of the Kapuskasing (Ontario) migmatitic mafic granulites by dehydration melting of amphibolite: The importance of quartz to the reaction progress. *Journal of Metamorphic Geology*, **14,** 591–611.

Inger, S. & Harris, N. B. W., 1992. Tectonothermal evolution of the High Himalayan crystalline sequence, Langtang Valley, northern Nepal. In: Metamorphic styles in young and ancient orogenic belts. (eds Pattison David, R. M., Ghent, E. D. & Gordon, T. M.) *Journal of Metamorphic Geology*, pp. 439–452.

Inger, S. & Harris, N., 1993. Geochemical constraints on leucogranite magmatism in the Langtang Valley, Nepal Himalaya. *Journal of Petrology*, **34,** 345–368.

Kirby, S. H. & Kronenberg, A. K., 1984. Deformation of clinopyroxenite: evidence for a transition in flow mechanisms and semi-brittle behavior. *Journal of Geophysics Research*, **89,** 3177–3192.

Kretz, R., 1983. Symbols for rock-forming minerals. *American Mineralogist*, **68,** 277–279.

Kronenberg, A., Kirby, S. & Pinkston, J., 1990. Basal slip and mechanical anisotropy of biotite. *Journal of Geophysical Research*, **95,** 19257–19278.

Le Fort, P., Cuney, M., Deniel, C., France-Lanord, C., Sheppard, S., Upreti, B., N., & Vidal, P., 1987. Crustal generation of Himalayan leucogranite. *Tectonophysics*, **134,** 39–57.

Mares, V. & Kronenberg, A., 1993. Experimental deformation of muscovite. *Journal of Structural Geology*, **15,** 1061–1075.

Milord, I., Sawyer, E. W. & Brown, M., 2001. Formation of diatexite migmatite and granite magma during anatexis of semi-pelitic metasedimentary rocks: an example from St. Malo, France. *Journal of Petrology*, **42,** 487–505.

Montel, J. M. & Vielzeuf, D., 1997. Partial melting of metagreywackes; Part II, Compositions of minerals and melts. *Contribution to Mineralogy and Petrology*, **128,** 176–196.

Nyman, M., Pattison, D. & Ghent, E., 1995. Melt extraction during formation of k-feldspar and sillimanite migmatites, west of Revelstoke, British Columbia. *Journal of Petrology*, **36,** 351–372.

Oliver, N. & Barr, T., 1997. The geometry and evolution of magma pathways through migmatites of the Halls Creek Orogen. *Western Australia. Mineralogical Magazine*, **61,** 3–14.

Patiño-Douce, A. & Harris, N., 1998. Experimental constraints on Himalayan anatexis. *Journal of Petrology*, **39,** 689–710.

Patino, D. A. E. & Beard, J. S., 1995. Dehydration-melting of biotite gnesis and quartz amphibolite from 3 to 15 kbar. *Journal of Petrology*, **36,** 707–738.

Pattison, D. R. M. & Harte, B., 1988. Evolution of structurally contrasting anatectic migmatites in the 3-kbar Ballachulish aureole, Scotland. *Journal of Metamorphic Geology*, **6,** 475–494.

Petford, N., Cruden, A. R., McCaffrey, K. J. W. & Vigneresse, J.-L., 2000. Granite magma formation, transport and emplacement in the Earth's crust. *Nature*, **408,** 669–673.

Pickering, J. & Johnston, A., 1998. Fluid-absent melting behavior of a two-mica metapelite: experimental constraints on the origin of black hills granite. *Journal of Petrology*, **39,** 1787–1804.

Rapp, R. P. & Watson, E. B., 1995. Dehydration melting of metabasalt at 8–32 kbar; implications for continental growth and crust-mantle recycling. *Journal of Petrology*, **36,** 891–931.

Rosenberg, C. & Riller, U., 2000. Partial melt topology in statically and dynamically recrystallized granite. *Geology*, **28,** 7–10.

Rushmer, T., 1991. The chemical and rheological behavior of partially molten amphibolite rocks. *PhD Thesis,* Swiss Federal Institute of Technology, Zurich.

Rushmer, T., 1995. An experimental deformation study of partially molten amphibolite: applications to low-fraction melt segregation. *Journal of Geophysical Research*, **100,** 15681–15696.

Rushmer, T., 2001. Volume change during partial melting reactions: implications for melt extraction, melt geochemistry and crustal rheology. *Tectonophysics*, **342,** 389–405.

Rutter, E., 1997. The influence of deformation on the extraction of crustal melts: a consideration of the role of melt-assisted granular flow. In: *Deformation-Enhanced Melt Segregation and Metamorphic Fluid Transport* (ed. Holness, M.), pp. 82–110. Chapman & Hall, London.

Rutter, E. & Neumann, D., 1995. Experimental deformation of partially molten Westerly granite under fluid-absent conditions, with implications for the extraction of granitic magmas. *Journal of Geophysical Research*, **100,** 15697–15715.

Sawyer, E. W., 1987. The role of Partial melting and fractional crystallization in determining discordant migmatite leucosome compositions. *Journal of Petrology*, **28,** 445–473.

Sawyer, E. W., 1991. Disequilibrium melting and the rate of melt-residuum separation during migmatisation of mafic rocks from the Grenville Front, Quebec. *Journal of Petrology*, **28,** 701–738.

Sawyer, E., 1998. Formation and evolution of granite magmas during crustal reworking: the significance of diatextites. *Journal of Petrology*, **39,** 1147–1167.

Sawyer, E., 2001. Melt segregation in the continental crust: distribution and movement of melt in anatectic rocks. *Journal of Metamorphic Geology*, **19,** 291–309.

Sawyer, E., Dombrowski, C. & Collins, W. J., 1999. Movement of melt during synchronous regional deformation and granulite-facies anatexis, an example from the Wuluma Hills, central Australia. In: *Understanding Granites; Integrating New and Classical Techniques, Special Publication, 158* (eds Castro, A., Fernandez, C. & Vigneresse, J.-L.), pp. 221–237. Geological Society, London.

Scaillet, B., France-Lanord, C. & Le Fort, P., 1990. Badrinath-Gangotri plutons (Garhwal, India): petrological and geochemical evidence for fractionation processes in a high Himalayan leucogranite. *Journal of Volcanological Research*, **44,** 163–188.

Shea, W. & Kronenberg, A., 1993. Strength and anisotropy of foliated rocks with varied mica contents. *Journal of Structural Geology*, **15,** 1097–1121.

Solar, G. S. & Brown, M., 2001. Petrogenesis of migmatites in Maine, USA: possible source of peraluminous leucogranite in plutons? *Journal of Petrology*, **42,** 789–823.

Troeger, L., Antignano, A., Holyoke, C. & Rushmer, T., 2001. Foliation orientation and strain rate controls on strength of pelite during partial melting and deformation. *Northeastern GSA, Abstracts with Programs*, **33,** A12.

Tullis, J. & Wenk, R., 1994. Effect of muscovite on the strength and lattice preferred orientations of experimentally deformed quartz aggregates. *Materials Science and Engineering*, **A175,** 209–220.

Vanderhaege, O. & Teyssier, C., 1997. Formation of the Shuswap metamorphic complex during late-orogenic collapse of the Canadian Cordillera: role of ductile thinning and partial melting of the mid- to lower crust. *Geodynamica Acta*, **10,** 41–58.

Vielzeuf, D. & Holloway, J., 1988. Experimental determination of the fluid-absent melting relations in the pelitic system: consequences for crustal differentiation. *Contributions to Mineralogy and Petrology*, **98,** 257–276.

Watson, E. B., Vicenzi, E. P. & Rapp, R. P., 1996. Inclusion/host relations involving accessory minerals in high grade metamorphic and anatectic terrains. *Contributions to Mineralogy and Petrology*, **101,** 220–231.

Watt, G. R., Burns, I. M. & Graham, G. A., 1996. Chemical characteristics of migmatites: accessory phase distribution and evidence for fast melt segregation rates. *Contributions to Mineralogy and Petrology*, **125,** 100–111.

Watt, G., Oliver, N. & Griffin, B. J., 2000. Evidence of reaction-induced microfracturing in granulite facies migmatites. *Geology*, **28,** 327–330.

Weber, C. & Barbey, P., 1986. The role of water, mixing processes and metamorphic fabric in the genesis of the Baume migmatites (Ardeche, France). *Contributions to Mineralogy and Petrology*, **92,** 481–491.

Weber, C., Barbey, P., Cuney, M. & Martin, H. 1985. Trace element behaviour during migmatization. Evidence for a complex melt–residuum–fluid interaction in the St. Malo migmatite dome (France). *Contributions to Mineralogy and Petrology*, **90,** 52–62.

Received 5 September 2000; revision accepted 14 January 2002.